CDD*press*

Check for updates

ARTICLE

The bone–liver interaction modulates immune and hematopoietic function through Pinch-Cxcl12-Mbl2 pathway

Tailin He[1,8], Bo Zhou[1,8], Guohuan Sun[2,8], Qinnan Yan[1], Sixiong Lin[3], Guixing Ma[1], Qing Yao[1], Xiaohao Wu[1], Yiming Zhong[1], Donghao Gan[1], Shaochuan Huo[4], Wenfei Jin[5], Di Chen[6], Xiaochun Bai[7✉], Tao Cheng[2✉], Huiling Cao[1✉] and Guozhi Xiao[1✉]

Mesenchymal stromal cells (MSCs) are used to treat infectious and immune diseases and disorders; however, its mechanism(s) remain incompletely defined. Here we find that bone marrow stromal cells (BMSCs) lacking Pinch1/2 proteins display dramatically reduced ability to suppress lipopolysaccharide (LPS)-induced acute lung injury and dextran sulfate sodium (DSS)-induced inflammatory bowel disease in mice. Prx1-Cre; Pinch1[f/f]; Pinch2^{−/−} transgenic mice have severe defects in both immune and hematopoietic functions, resulting in premature death, which can be restored by intravenous injection of wild-type BMSCs. Single cell sequencing analyses reveal dramatic alterations in subpopulations of the BMSCs in Pinch mutant mice. Pinch loss in Prx1^{+} cells blocks differentiation and maturation of hematopoietic cells in the bone marrow and increases production of pro-inflammatory cytokines TNF-α and IL-1β in monocytes. We find that Pinch is critical for expression of Cxcl12 in BMSCs; reduced production of Cxcl12 protein from Pinch-deficient BMSCs reduces expression of the Mbl2 complement in hepatocytes, thus impairing the innate immunity and thereby contributing to infection and death. Administration of recombinant Mbl2 protein restores the lethality induced by Pinch loss in mice. Collectively, we demonstrate that the novel Pinch-Cxcl12-Mbl2 signaling pathway promotes the interactions between bone and liver to modulate immunity and hematopoiesis and may provide a useful therapeutic target for immune and infectious diseases.

INTRODUCTION

Mesenchymal stromal/stem cells (MSCs) are multipotent cells which have the ability to differentiate into multiple cell types, including chondrocytes, osteoblasts, adipocytes, and muscle cells [1]. MSCs can be obtained from bone marrow, adipose tissue, umbilical cord, and other tissue/organs [2]. In addition to their regenerative properties, MSCs have a strong immunoregulatory potential [3]. They were shown to inhibit T cell, B cell and NK cell activation and proliferation and suppress the migration and maturation of antigen-presenting cells (APCs). MSCs, as one of the most pivotal components of the bone marrow microenvironment, play a crucial role in regulating the homing, proliferation, and differentiation of hematopoietic stem cells (HSCs). Hematopoiesis in bone marrow is in charge of generating major lineages of innate effectors, such as NK cells, granulocytes, monocytes and dendritic cells [4]. As various types of immune cells are differentiated from HSCs, damage associated with their integrity

could threaten downstream immune responses, which may cause life-threatening infections and sepsis [5]. Presently, no specific treatment is available for sepsis and septic shock. Cell-based immunotherapies can provide safe and effective treatments for excessive pro-inflammatory events in infections [6]. MSCs display various beneficial properties against infectious diseases, driven by their paracrine effects through trophic factors which have anti-fibrotic, anti-apoptotic, or pro-angiogenic effects [7–9]. As cellular pharmaceuticals, MSCs are potent modulators of immune responses and have been utilized for the treatment of ischemic, inflammatory, and immunological disorders [10, 11]. MSCs anchor at injured tissues or organs and promote macrophages to regulate inflammatory cytokines and secrete paracrine factors to inhibit systemic and local inflammation. MSCs reprogram monocytes/ macrophages by releasing prostaglandin E2 (PGE2) that acts on the macrophages to stimulate IL-10 secretion, exerting the anti-inflammatory effects and attenuating sepsis in mice [12].

[1]Department of Biochemistry, School of Medicine, Southern University of Science and Technology, Guangdong Provincial Key Laboratory of Cell Microenvironment and Disease Research, Shenzhen Key Laboratory of Cell Microenvironment, Shenzhen 518055, China. [2]State Key Laboratory of Experimental Hematology, National Clinical Research Center for Blood Diseases, Haihe Laboratory of Cell Ecosystem, Institute of Hematology & Blood Diseases Hospital, Chinese Academy of Medical Sciences & Peking Union Medical College, Tianjin, China; CAMS Center for Stem Cell Medicine, PUMC Department of Stem Cell and Regenerative Medicine, Tianjin, China. [3]Guangdong Provincial Key Laboratory of Orthopaedics and Traumatology, Department of Spine Surgery, The First Affiliated Hospital of Sun Yat-sen University, Guangzhou, China. [4]Shenzhen Hospital of Guangzhou University of Chinese Medicine (Futian), Shenzhen, China. [5]Shenzhen Key Laboratory of Gene Regulation and Systems Biology, School of Life Sciences, Southern University of Science and Technology, Shenzhen 518055, China. [6]Research Center for Human Tissues and Organs Degeneration, Shenzhen Institutes of Advanced Technology, Chinese Academy of Sciences, Shenzhen 518055, China. [7]Guangdong Provincial Key Laboratory of Bone and Joint Degeneration Diseases, Department of Cell Biology, School of Basic Medical Sciences, Southern Medical University, Guangzhou, China. [9]These authors contributed equally: Tailin He, Bo Zhou, Guohuan Sun. ✉email: baixc15@smu.edu.cn; chengtao@ihcams.ac.cn; caohl@sustech.edu.cn; xiaogz@sustech.edu.cn

Transforming growth factor-beta1 (TGF-β1) is an important cytokine secreted by MSCs. It can switch the macrophage phenotype from pro-inflammation to anti-inflammation and attenuate organ dysfunction by reducing macrophage-driven inflammation in septic mice [13]. The CXCL12 ligand (also known as stromal cell-derived factor 1 [SDF1] and CXCR4 receptor have been well investigated for their role in cell survival, migration, and invasion by triggering multiple signal transduction pathways [14]. Cxcl12 secreted by MSCs is a crucial homeostatic chemokine that controls hematopoietic cell trafficking and adhesion in various pathological processes [15, 16]. However, the detailed immuno-modulatory mechanisms of chemokines provided by MSCs remain poorly defined. That is, there is still a gap between basic and clinical research, indicating a need for exploring innovative therapeutic targets to enhance the effectiveness of MSC-based therapies.

Focal adhesions (FAs) are vital mechanical linkages that connect the extracellular matrix (ECM) and cytoskeleton, allowing for crucial cell-environment communication [17]. They modulate various physiological processes, including cell attachment, migration, differentiation, and mechanotransduction [17]. Recent studies have highlighted the essential roles of FA proteins in inflammatory-related illnesses. Specifically, Kindlin-2 loss in nucleus pulposus cells activates Nlrp3 inflammasome, inducing IL-1β expression in mice [18]. The removal of Kindlin-2 in articular chondrocytes results in the development of spontaneous osteoarthritis (OA) and exacerbates instability-induced OA lesions in adult mice [19]. Moreover, the deletion of Kindlin-2 in hepatocytes activates the tumor necrosis factor (TNF) pathway, ultimately leading to severe inflammatory liver disease and premature death [20]. PINCH proteins, including PINCH1 and PINCH2, are major FA proteins expressed throughout most tissues and organs [21]. In our previous study, we found that ablation of Pinch1/2 in Prx1+ cells (primarily mesenchymal stem cells) severely reduced chondrocyte proliferation and promoted chondrocyte differentiation and hypertrophy, leading to dwarfism and severe osteopenia [22]. The elimination of Pinch1/2 in aggrecan+ cells resulted in degenerative disc disease and an increase in the secretion of TNF-α [23]. Given the influential role of FA proteins in inflammatory diseases, we ought to investigate the further mechanisms to understand the roles of FA proteins.

Mannose-binding lectin (MBL) is a C-type serum lectin that binds to microbial surface carbohydrates, activating the lectin complement pathway [24, 25]. Research has shown a correlation between low MBL levels and bacterial infections, meningococcal sepsis, and HIV infection [26, 27]. MBL supplementation offers potential applications to prevent infection in humans but requires careful clinical study. Understanding the concrete mechanisms regulating MBL expression would facilitate the development of its local or systemic therapeutic approaches.

In this study, we demonstrate a critical role of BMSC Pinch proteins in control of immune and hematopoietic functions in mice. We demonstrate that the abilities of MSCs to treat inflammatory diseases in two mouse disease models are largely dependent upon the presence of the Pinch proteins in these cells. Deleting Pinch expression in Prx1+ cells impairs both immune and hematopoietic function and promotes inflammation in mice. We demonstrate that the crosstalk between the bone and liver modulates immunity and hematopoiesis at least in part through the Pinch-Cxcl12-Mbl2 pathway.

RESULTS
Pinch loss causes multiple organ and tissue lesions in mice
Our previously published studies showed that deleting Pinch1/2 in the Prx1+ cells resulted in premature deaths in mice [22]; the underlying cause(s) were not defined. We found that the Pinch1/2 double knockout mice, we were generated as described in Fig.

S1A, B and referred to as dKO hereafter, developed severe subcutaneous hematoma 4 to 6 weeks after birth (Fig. 1A). dKO mice had reduced blood perfusion in the liver and kidney, accompanied with higher spleen index (Fig. 1B). Moreover, Pinch loss markedly reduced the cellularity in the bone marrow of the long bones (Fig. 1C).

Pinch modulates osteogenic, chondrogenic and immune-regulatory pathways in bone marrow stroma
We performed 10X scRNA-seq on Lepr+ cells sorted from control and dKO mice to investigate the changes of bone marrow stromal cells after Pinch loss, especially BMSCs. We merged scRNA-seq data from control and dKO samples and identified 15 clusters based on their gene expression (Fig. S2A–C). Among these cells, three clusters (3,11,12) expressed Tfrc, Hba-a1, Car1, or Pf4 at high level, indicating they were erythroblasts (cluster 3), erythrocytes (cluster 11) or megakaryocytes (cluster 12) (Fig. S2D). Proportion of erythroblasts and erythrocytes was increased and proportion of megakaryocytes was decreased in dKO group compared to those in control group (Fig. S2E). The expression of Gfi1b, Klf3, and Myb, transcription factors involved in hematopoiesis, was down-regulated in dKO group relative to that in control group (Fig. S2F). We used 15539 cells in other 12 clusters for subsequent analyses. These cells were grouped into 22 clusters and assigned as eight major cell types: Lepr+ BMSC (Lepr, Cxcl12, Adipoq, Vcam1, Kitl, Rarres2), osteoprogenitor cells (Runx2, Sp7, Alpl, Spp1), osteoblasts (Bglap, Col1a1), chondrocytes (Sox9, Acan, Col2a1, Col9a1), adipocytes (Adipoq, Fabp4), endothelial cells (Cdh5, Pecam1, Kdr, Cd34, Eng, Emcn), fibroblasts (Dcn, Clec3b, Myoc), and pericytes (S100a4, Acta2, Myh11) (Fig. 1D, E, S3A–C and S4A–C). Furthermore, cluster 18 expressed high level of Wnt2 and Rorb. Interestingly, these cells were observed in only dKO group; their identity was not determined. Although we used sorted Lepr+ cells for scRNA-seq, we only observed high expression of Lepr in several clusters, which were annotated as Lepr+ BMSC (Fig. S3B). For Prx1, we found this gene was expressed at not only Lepr+ BMSCs but also at a limited number of osteoblasts, chondrocytes, pericytes, endothelial, and fibroblasts, indicating that Pinch1 was deleted in all these cells (Fig. S3B). However, Pinch1 is mainly distributed in BMSCs and pericytes, while Prx1 is mainly distributed in BMSCs and osteoblasts, so that the knockout efficiency of Pinch1 in MSCs is acceptable (Fig. S5A–H). Around 67% of Prx1+ cells express Pinch1 while only 8.77% of them express Pinch2. The rates of Lepr+ cells also expressing Pinch1 or Pinch2 are 67.94% and 5.04%, respectively. In addition, 65.5% of Prx1+ and Pinch1+ double positive cells are Lepr+ BMSCs. However, we could not overlook the expression of Pinch2. It has been reported that, although Pinch2 KO mice do not show apparent phenotypes, there is a functional redundancy between Pinch1 and Pinch2 [28].

Among cells in the 22 clusters, Lepr+ BMSCs accounted for about 48% in control group; this number was reduced to about 19% in KO group (Fig. 1F). Additionally, proportion of both osteoblasts and adipocytes was decreased in dKO group compared to that in control group, while proportion of both fibroblasts and pericytes was dramatically increased in dKO group compared to that in control group (Fig. 1F). In t-SNE visualization, we found that cells in one Lepr+ BMSC cluster (2) and two pericytes clusters (3, 5) were almost exclusively identified in dKO group; they were barely observed in control group (Fig. 1E). Cells in two clusters of Lepr+ BMSC (0, 1) were mostly from control group. To investigate the proportion of each cell type in greater detail, we next analyzed proportion of sub-clusters for the cell types with multiple clusters as described in Fig. 1F. We found that proportion of sub-clusters in several cell types between control and KO was distinct, including Lepr+ BMSCs, fibroblasts, chondrocytes, endothelial cells, and pericytes. For Lepr+ BMSCs, we initially classified them into 4 clusters (0, 1, 2, 15), cells in
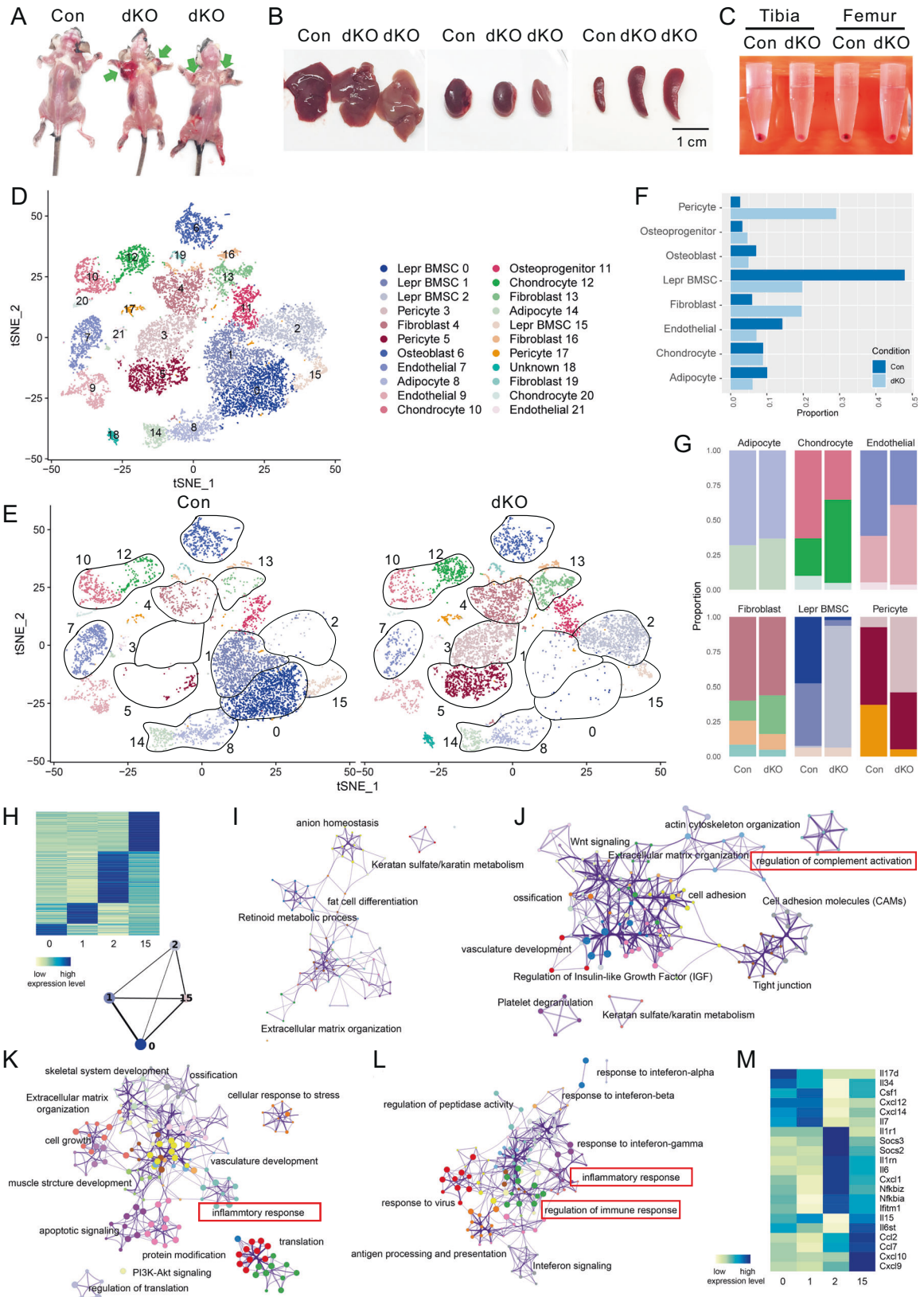
clusters 0 and 1 were mainly found in control group and cells in cluster 2 were mainly found in dKO group. Among three chondrocytes clusters, cluster 10 accounted for about 63% chondrocytes in control group, while it comprised only about

35% in dKO group. We found that cluster 12 comprised about 27% chondrocytes in control group but about 63% chondrocytes in dKO group (Fig. 1G). Among three endothelial cells clusters, cluster 7 comprised most endothelial cells in control group and

Fig. 1 Pinch1^{Prx1}; Pinch2$^{-/-}$ (dKO) mice display abnormal appearance, cell population structure and gene expression patterns. A Representative pictures of 6-wk-old male control (Pinch1$^{f/f}$; Pinch2$^{-/-}$), and Pinch1^{Prx1}; Pinch2$^{-/-}$ (dKO) mice removing the skin. **B** Representative pictures of organs from 6-wk-old male control and dKO mice. Scale bar, 1 cm. **C** Whole bone marrow cells of the tibia or femur from control and dKO mice. Visualization of bone marrow Lepr$^+$ cells in UMAP. Lepr$^+$ cells from control group and dKO group were visualized together (**D**) or separately (**E**). Cells were colored by their clusters. **F** Cell proportion of major cell types in control group and dKO group. **G** Proportion of each cluster in each major cell type in control group and dKO group. Color of each cluster was indicated as in (**D**). **H** Expression of top differential genes and connectivity analysis in each Lepr$^+$ BMSCs clusters. Functional enrichment analysis using differentially expressed genes (absolute log2 fold change >0.2) between control group and dKO group for cluster 0 (**I**), cluster 1 (**J**) cluster 2 (**K**), and cluster 15 (**L**). **M** Expression of immune response related genes across four Lepr$^+$ BMSCs clusters.

cluster 9 comprised most endothelial cells in dKO group (Fig. 1G). For fibroblasts, proportion of cluster 13 was increased in dKO group compared to that in control group; proportion of both clusters 16 and 19 was decreased in dKO group compared to that in control group (Fig. 1G). For pericytes, proportion of cluster 3 was increased in dKO group compared to that in control group; proportion of clusters both 5 and 17 was decreased in dKO group compared to that in control group (Fig. 1G).

We observed distinct gene expression patterns in the four clusters assigned as Lepr$^+$ BMSC (0,1,2, and 15) (Fig. 1H). Connectivity of the four clusters revealed that cluster 0 and cluster 1 were strongly connected, while cluster 2 showed much weaker connectivity with other three clusters (Fig. 1H). We next conducted functional analysis for these sub-clusters of Lepr$^+$ BMSC using highly expressed genes in each cluster. We found that retinoid metabolic process and fat cell differentiation related terms were enriched in cluster 0 (Fig. 1I). Bone formation, vasculature structure development, and complement activation related terms were enriched in cluster 1 (Fig. 1J). Bone formation, vasculature structure development, inflammatory response, and apoptosis related terms were enriched in cluster 2 (Fig. 1K). Inflammatory response, interferon signaling, and antigen processing and presentation related terms were enriched in cluster 15 (Fig. 1L). In a word, cluster 2 and 15 are highly related to inflammation, elevation of which in dKO mice might contribute to the dysfunction of immune regulatory and hematopoietic functions. Expression of genes involved in adipogenesis (Fig. S4D), ossification (Fig. S4E), vasculature development (Fig. S4F), Wnt signaling pathway (Fig. S4G), and extracellular matrix organization related genes (Fig. S4H) was altered in cluster 2 compared to that in other three clusters. We found that cytokines and other immune related genes were significantly differentially expressed in the four clusters, indicating that communication between Lepr$^+$ BMSCs and immune cells was dramatically altered by Pinch loss (Fig. 1M). We performed differential analysis for Lepr$^+$ BMSCs between control group and dKO group and found that the expression levels of transcription factors *Snai2*, *Foxc1* that involved in regulation of Cxcl12, and adipogenesis related transcription factor *Cebpa* were down-regulated in dKO group compared to those in control group (Fig. S4I). Expression levels of vasculature structure development related transcription factors *Epas1*, *Myc*, *Nr4a1*, *Nr4a3*, *Arid5b* were up-regulated in dKO group compared to those in control group. Expression of *Cebpd*, a transcription factor involved in regulation of Il6, was up-regulated in dKO group compared to that in control group (Fig. S4I).

Considering the dramatic alteration in BMSCs due to Pinch loss in Prx1$^+$ cells, we performed a number of experiments to determine the FA formation, migration, proliferation, and differentiation abilities of BMSCs in vitro. Primary BMSCs were isolated from control and dKO mice. With this broad influence in FA and FA-associated proteins, Pinch deletion in Prx1$^+$ cells affected the FA formation and cellular morphology in BMSCs. The removal of Pinch resulted in dramatic changes in FA, characterized by looser and less-concentrated attachment to the substrate, indicating reduced tension in the Pinch knockout FA sites (Fig. S6A–C). Additionally, Pinch deletion also caused noticeable morphological changes in BMSCs, including significant reductions in nuclear size

and spreading area (Fig. S6A–C). The scratch assay results revealed that the migration ability of BMSCs was decreased in dKO group (Fig. S6D, E). To determine whether Pinch loss in Prx1$^+$ cells impacts the proliferation capacity, we performed CCK-8 assay and found that dKO BMSCs displayed defective proliferation capacity (Fig. S6F). When induced towards osteogenic differentiation, dKO BMSCs showed a significant decrease in the expression of runt-related transcription factor 2 (*Runx2*), osterix (*Osx*), alkaline phosphatase (*Alp*), collagen typeI alpha1 (*Col1a1*), bone sialoprotein (*Bsp*), and osteocalcin (*Ocn*) mRNAs, indicating decreased osteoblastic capacity. (Fig. S6G). Collectively, these results suggest that Pinch deletion in Prx1$^+$ cells impairs focal adhesion formation, migration, proliferation, and differentiation of BMSCs.

We further conducted functional analyses for the remaining cell types. Results showed that ossification, cartilage development, extracellular matrix organization, skeletal system development related terms were enriched in cluster 10 (chondrocytes) (Fig. S7A). In addition, metabolism, translation, protein folding, mitochondrion organization, and apoptosis related terms were also significantly enriched in cluster 10. We found Wnt signaling pathway, BMP signaling pathway and TGFB signaling pathway related terms were enriched in cluster 12 (Fig. S7B). Platelet degranulation was enriched in cluster 12. Cluster 20 was a group of chondrocytes with high proliferation activity, which was indicated by these cell cycle related terms (Fig. S7C). For pericytes, actin cytoskeleton organization, extracellular matrix organization and cell adhesion related terms were enriched in clusters 3 and 5, cell cycle related terms were enriched in cluster 17 (Fig. S7D–F). Clusters of endothelial cells showed different patterns of hemostasis since hemostasis related terms were significant in both cluster 7 and cluster 9, but not cluster 21 (Fig. S7G–I). Thus, hemostasis was significantly regulated. Besides, we compared the functions of fibroblasts sub-clusters (cluster 4, 13, 16, 19) and cluster 18, similar terms were enriched in these clusters (Fig. S7J–N). Thus, these dramatic gene alterations in various cell types due to Pinch loss in Prx1$^+$ cells ultimately caused severe chondrodysplasia and osteopenia with subtle limb shortening, which has been reported in our previous study [22]. Moreover, above results gave us novel insights into investigating the immune regulatory and hematopoietic role of Pinch in MSCs further.

Pinch loss impairs hematopoiesis in mice

As dKO mice developed hemorrhagic diathesis, we assessed their coagulation functions. Tail bleeding time assay (Fig. 2A) showed that that dKO mice displayed significantly prolonged blood clotting time. The red blood cell count (RBC) and platelet count from the peripheral blood were dramatically decreased in dKO mice compared to those in their littermate controls (Fig. 2B, C). In addition, lymphocyte count (Fig. 2D) was diseased and neutrophil count (Fig. 2E) and monocyte count (Fig. 2F) were significantly increased in dKO mice, suggesting the presence of infection and immune dysfunction.

Using flow cytometry analysis, we found that the numbers of CD3$^+$/B220$^-$ T cells, CD3$^-$/B220$^+$ B cells, and Ter119$^+$ erythroid cells were all remarkably decreased and that the number of Ter119$^-$/Mac-1$^+$/Gr-1$^+$ granulocytes was increased in dKO mice
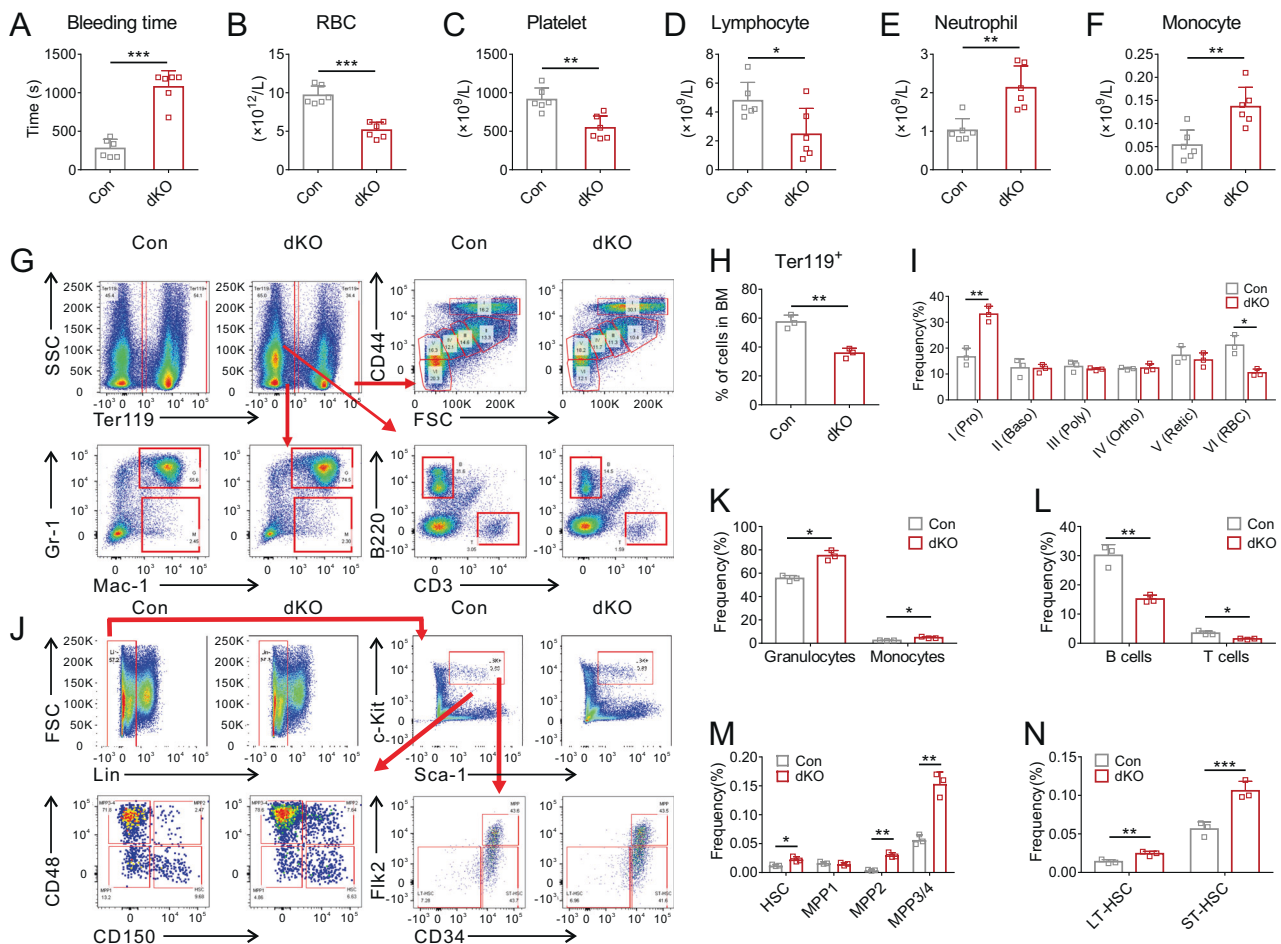
Fig. 2 Pinch loss dramatically altered hematopoietic progenitors and linages. A Tail bleeding time measured in control and dKO mice ($n = 6$). **B–F** Routine blood examination of 6-wk-old male control and dKO mice ($n = 6$). **G–N** FACS analysis of bone marrow cells in 6-wk-old male control and dKO mice ($n = 3$). Data are mean ± SD of 3 independent experiments. *$P < 0.05$; **$P < 0.01$; ***$P < 0.001$.

(Fig. 2G–L). Strikingly, the maturation process of erythrocytes was hampered, as demonstrated by increased proerythroblast cells and decreased mature red blood cells in dKO versus control mice (Fig. 2I). Next, we examined the differentiation of the hematopoietic cells (Fig. 2J–N). Among 4 subtypes of multipotent progenitor cells (MPP), the numbers of both Lin$^-$/Sca1$^+$/c-Kit$^+$/CD150$^+$/CD48$^+$ MPP2 cells, which produce platelets and erythrocytes, and MPP3/4 cells, which produce inflammatory immune cells, were significantly increased in cKO relative to those in control mice. In addition, the number of CD150$^+$/CD48$^-$ hematopoietic stem cells (HSCs), including CD34$^-$/Flk2$^-$ long-term hematopoietic stem cells (LT-HSCs) and CD34$^+$/Flk2$^-$ short-term hematopoietic stem cells (ST-HSCs), was elevated in dKO relative to control mice. Collectively, these results suggest that Pinch signaling from Prx1$^+$ cells plays a pivotal role in maintaining the normal hematopoietic and immune functions in mice.

Pinch loss reduces production of both innate and adaptive immune cells

Hematopoiesis in bone marrow is responsible for generation of major lineages of innate effectors, including monocytes, macrophages, NK cells, granulocytes, and dendritic cells. In adult mammals, hematopoiesis occurs primarily in the bone marrow, where hematopoietic stem cells (HSCs) and restricted hematopoietic progenitors are maintained throughout life. HSCs are maintained in a perivascular niche, in which Lepr$^+$ stromal cells and endothelial cells produce various factors for HSC maintenance, such as stem cell

factor (SCF) [29] and Cxcl12 [30]. To comprehensively investigate how Pinch loss impacts the bone marrow hematopoietic cells in vivo, we performed 10X single-cell RNA sequencing on suspension hematopoietic cells from the bone marrow of control and dKO mice. Total 33432 cells from the four samples (2 control mice and 2 dKO mice) passed quality control and were enrolled for subsequent integration analysis with Seurat (Fig. S8A). Single cell RNA sequencing data were embedded into low dimensional data and visualized in UMAP. Initially, we classified these cells into 32 clusters (Fig. S8B). They were next annotated to 14 cell types, including hematopoietic stem and progenitor cells (HSPCs), granulocyte monocyte progenitors (GMPs), neutrophil progenitors, immature neutrophils, mature neutrophils, monocyte precursors, monocytes, plasmacytoid dendritic cells (pDC), conventional dendritic cells (cDC), basophils, T cells, natural killer cells, B cells and erythrocytes, according to expression levels of well-known cell type specific genes and cell cycle score (Fig. 3A, Fig. S8C–E). Cluster 17, which was lineage negative cluster with relative high expression of *Cd34* and *Kit*, was identified as HSPC. Cluster 12 that expressed *Cd34*, *Csf1r* and primary granule proteins (*Hexa*, *Mpo*) was named as GMP. Based on expression levels of primary granules (*Hexa*, *Mpo*), secondary granules (*Ltf*, *Lyz2*), tertiary granules (*Mmp8*), other well-known neutrophilic related genes (*Cebpb*, *Ly6g*, *Il1b*, *Ccrl2*, *Cxcr2*) and cell cycle scores (G2M score, S score), neutrophilic lineage clusters (0, 1, 2, 3, 4, 7, 9, 10, 14, 20, 21, and 22) were identified and classified into three developmental stages (neutrophil progenitor, immature neutrophil, and mature neutrophil) (Fig. S8C–E). Monocytic lineage
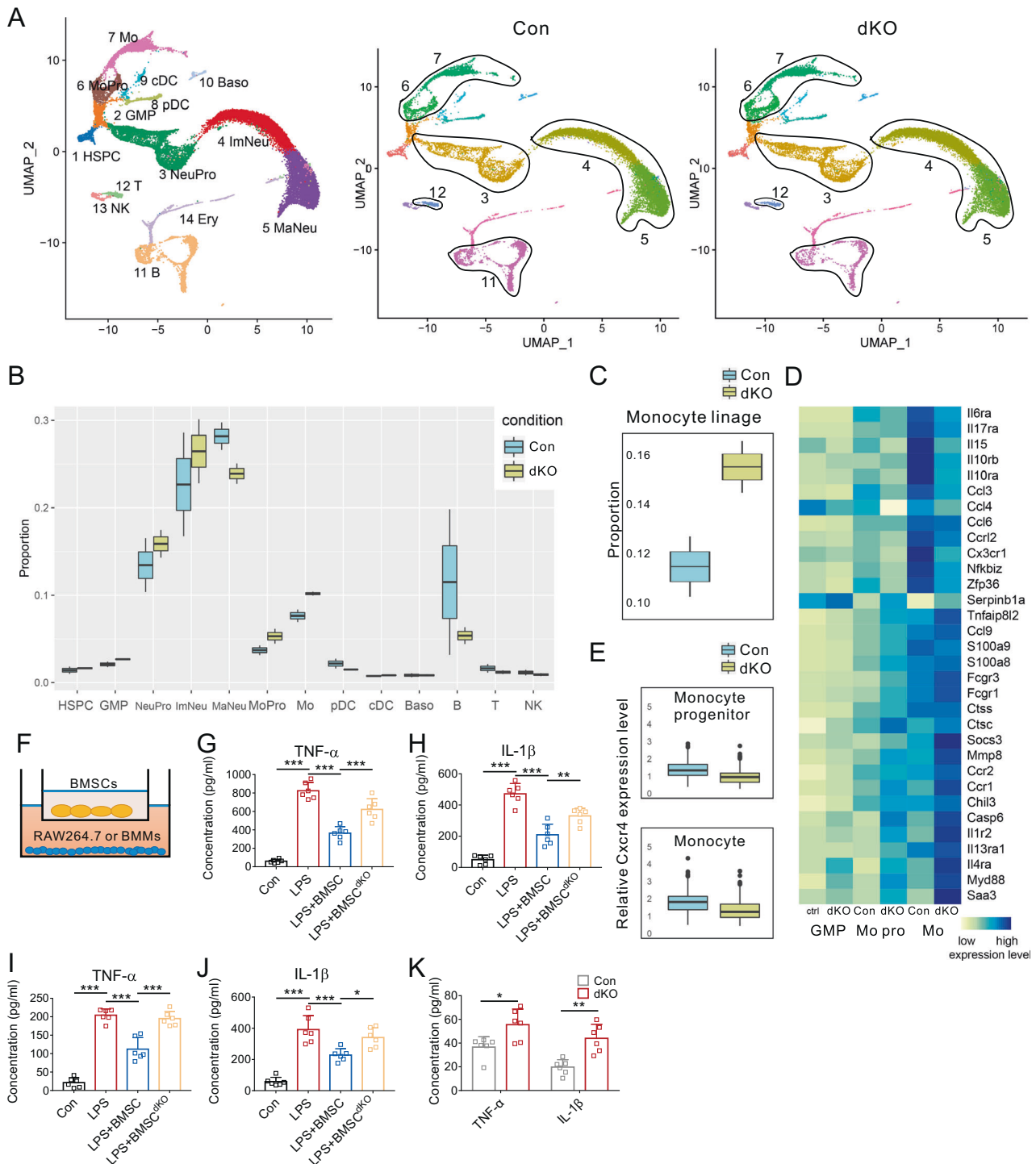
Fig. 3 Pinch loss significantly stimulates inflammatory response related genes in monocytes. A Visualization of bone marrow hematopoietic cells in 6-wk-old male control and dKO mice in UMAP using scRNA-seq. **B** Cell proportion of each cell type in 6-wk-old male control and dKO mice using scRNA-seq. **C** Cell proportion of monocyte lineage cells in control group and dKO group. **D** Expression levels of immune related genes in GMPs, monocyte progenitors (MoPro), and Monocytes (Mo) in 6-wk-old male control and dKO mice. **E** Expression level of *Cxcr4* in neutrophil progenitors, immature neutrophils, mature neutrophils, monocyte progenitors, and monocytes. **F** A diagram of co-culture system. BMSCs are seeded in the top wells, and RAW264.7 cells or primary bone marrow monocytes were seeded in the bottom wells, with pretreatment with or without LPS. TNF-α (**G**) and IL-1β (**H**) concentrations in the culture medium of RAW264.7 cells after co-cultured with BMSC or BMSC^{dKO} followed by LPS challenge ($n = 6$). Data are mean ± SD of 3 independent experiments. TNF-α (**I**) and IL-1β (**J**) concentrations in the culture medium of primary bone marrow monocytes after co-cultured with BMSC or BMSC^{dKO} followed by LPS challenge ($n = 6$). Data are mean ± SD of 3 independent experiments. **K** Serum TNF-α and IL-1β concentrations in 6-wk-old male control and dKO mice ($n = 6$). Data are mean ± SD of 3 independent experiments. *$P < 0.05$; **$P < 0.01$; ***$P < 0.001$.

clusters (5, 6, 18, 24, and 30) were identified via expression levels of monocytic related genes (*Csf1r*, *Cd68*, *Ccr2*, *Cx3cr1* and *Adgre4*). Cluster 6 was named as monocyte progenitor, according to its high cell cycle scores (Fig. S8C, D). Two clusters of dendritic cells (16, 27) were identified among these clusters by high expression levels of *H2-Aa*, *Siglech* (pDC), and *Cd209a* (cDC). Cluster 26 was identified as basophil as it expressed high level of *Mcpt8*. Cluster 19 was identified as T cell via expression levels of *Trbc2* and *Cd3g*. Cluster 23 was identified as natural killer cell (NK cell) via expression level of *Gzma*. B cells were identified via expression levels of *Cd79a*, *Ebf1*, *Vpreb1*, *Ms4a1* and *Iglv1* in clusters 8, 13, 15, 28, 29, and 31. Erythrocytes were identified via expression of the erythrocytes-related genes *Gypa* and *Hba-a1* in cluster 11 and 25 (Fig. S8E). To assess whether development of hematopoietic cells is impacted, we analyzed the bone marrow cell proportions in control and dKO mice (Fig. 3B). The results revealed that, when compared to control group, dKO group displayed markedly altered cell composition; dKO mice had higher proportion of HSPCs, GMPs, neutrophils and monocytes (Fig. 3B). Among all cells, proportion of neutrophil progenitors and immature neutrophils was higher in dKO group than that in control group. However, proportion of mature neutrophils in dKO group was lower than that in control group. Among all cells, the proportion of both monocyte progenitors and monocytes was increased in dKO group relative to that in control group. For composition of monocyte lineage cells and neutrophil linage cells, we found that proportion of monocyte progenitors, neutrophil progenitors and immature neutrophils was slightly increased in dKO group relative to that in control group (Fig. 3B). The proportion of monocyte lineage cells was dramatically increased in dKO versus control group (Fig. 3C). Among all cells, proportion of B cells, T cells, pDCs, and NK cells was decreased in dKO relative to control mice (Fig. 3B).

Pinch inhibits production of pro-inflammatory cytokines factors in monocytes

Wilcox test was employed to compare gene expression of control versus dKO groups for each cell type. Differentially and significantly regulated genes were observed in all cell types, especially in GMPs, monocyte progenitors, and monocytes (Figs. 3D and S9A). We observed dramatic alterations in expression of immune response related genes in GMPs, monocyte progenitors and monocytes dKO versus control groups. In GMPs, monocyte progenitors and monocytes. The expression of inflammatory-related genes, including *Chil3*, *Socs3*, *Ctsc*, *Fcgr1*, *Fcgr3*, *Mmp8*, *Myd88* and *Saa3*, was significantly up-regulated in dKO group compared to that in control group. For cytokines in GMPs, monocyte progenitors and monocytes, we found that *Ccl9* was up-regulated and *Il15*, *Ccl3*, *Ccl4*, *Ccl6* were down-regulated in dKO relative to control group. In GMPs, monocyte progenitors and monocytes, receptors *Ccr1*, *Ccr2*, *Il1r2*, *Il4ra*, *Il13ra1* were up-regulated and *Ccrl2*, *Cx3cr1*, *Il6ra*, *Il10ra*, *Il10rb*, *Il17ra* were down-regulated in dKO versus control groups (Fig. 3D). In monocyte lineage cells, *Cxcr4*, a major receptor of Cxcl12, was significantly down-regulated in dKO group compared to that in control group (Fig. 3E). Differential gene expression analysis revealed that *Cebpb*, an important transcription factor involved in hematopoiesis and inflammatory response, was up-regulated in GMPs in dKO group relative to control group (Fig. S9B). Interestingly, this transcription factor was down-regulated in monocyte progenitors, monocytes and mature neutrophils in dKO versus control groups. In B cells, we found transcription factors *Foxp1*, *Pax5*, *Rag1*, *Bach2* were down-regulated in dKO group compared to that in control group (Fig. S9B). In several cell types, transcription factors *Atf3*, *Fos*, *Fosb*, *Jun*, *Junb*, *Jund*, *Klf2*, *Klf4*, *Klf6*, *Tsc22d3*, and *Zfp36l2* were down-regulated in dKO group compared to that in control group (Fig. S9B). In monocyte progenitors and monocytes, transcription factors *Xbp1* and *Plscr1* were up-regulated in dKO versus control group (Fig. S9B). In immature neutrophils and neutrophils, transcription factor *Klf13* was up-regulated in dKO group compared to that in control group (Fig. S9B). Functional enrichment analysis using differentially expressed

genes between dKO and control group revealed that inflammatory response, cytokine production and apoptosis related terms were significantly enriched in GMPs, monocyte progenitors, monocytes and mature neutrophils (Fig. S9C–F). Mitochondrion organization and mitochondrion translation related terms were significantly enriched in only GMPs (Fig. S9C). Antigen processing and presentation related terms were significantly enriched in only mature neutrophils (Fig. S9D). Reactive oxygen species (ROS) related terms were significantly enriched in only mature neutrophils (Fig. S9F).

We cultured primary bone marrow stromal cells (BMSCs) with either a macrophage cell line RAW264.7 or primary bone marrow monocytes (BMMs) in the transwell system (Fig. 3F). The results showed that LPS dramatically induced production of TNF-α and IL-1β proteins in both RAW264.7 cells (Fig. 3G, H) or primary BMMs (Fig. 3I, J), which was significantly suppressed by wild-type BMSCs. However, the loss of Pinch reduced the ability of BMSCs to suppress the LPS-induced production of TNF-α and IL-1β in both cells. In vivo, we found that the levels of TNF-α and IL-1β were significantly higher in dKO than in control mice (Fig. 3K).

Intravenous injection of BMSCs prevents the hematopoietic defects and lethality induced by Pinch deficiency in mice

We next administrated BMSCs intravenously into dKO mice to investigate whether defects induced by Pinch deficiency in dKO mice can be rescued after MSC therapy. First, we determined the survival rate of dKO mice untreated or treated with wild-type BMSCs. There was a statistically significant improvement in the survival of dKO mice administrated with intravenous BMSCs on the 4 weeks after birth; around 40% of dKO mice treated with BMSCs survived while all the dKO mice without BMSC treatment sacrificed after 10 weeks of birth (Fig. 4A). The beneficial effect on survival could be seen from the body weight of the mice. The body weight of dKO mice treated with BMSCs increased steadily while those without treatment showed a decreasing trend (Fig. 4B, C). We also observed the limbs of dKO mice treated with BMSCs. As shown in Fig. 4D, the severe hematoma relieved after the age of 2 months and started to form scabs and crusts, which turned out to be normal on the 4th month. We evaluated inflammatory cytokines in serum, including TNF-α and IL-1β. Results showed that BMSC treatment significantly decreased the levels of both cytokines in dKO mice (Fig. 4E). As shown in Fig. 4F, the liver, kidney, and spleen tended to be normal 2 months after BMSC treatment. The reduced bone marrow cellularity in cKO mice was markedly restored after BMSC treatment for 2 months (Fig. 4G). The bleeding time of dKO mice was reduced after BMSC treatment (Fig. 4H). The red blood cell count and platelet count were elevated (Fig. 4I, J). Lymphocyte count (Fig. 4K) was increased while neutrophil count (Fig. 4L) and monocyte count (Fig. 4M) were significantly decreased in dKO mice with BMSC administration. We extracted the bone marrow cells from dKO mice administrated with BMSCs 2 months after treatment and evaluated the number of HSCs, MPPs, erythrocytes, granulocytes, macrophages, T cells, and B cells by flow cytometry (Fig. 4N, O). After BMSC treatment, the numbers of LT-HSCs (Fig. 4P), ST-HSCs (Fig. 4Q) and MPPs (Fig. 4R) turned out to be normal. Erythrocytes (Fig. 4S), T cells (Fig. Fig. 4), and B cells (Fig. 4U) were increased, and granulocytes (Fig. 4V) were decreased by BMSC treatment.

Pinch regulates hematopoietic and immunoregulatory function by modulating the Mbl2-mediated complement pathway

To further elucidate the mechanism of the vital role of Pinch in BMSCs, we collected the bone marrow cells and supernatants from the femurs of dKO mice and their control littermates, followed by liquid chromatography-tandem mass spectrometry (LC–MS/MS) to assess differentially expressed proteins of bone marrow from the two genotypes. Quality control of the samples was passed and the accuracy of FDR was set as 1% (Fig. S10A). The protein containing at
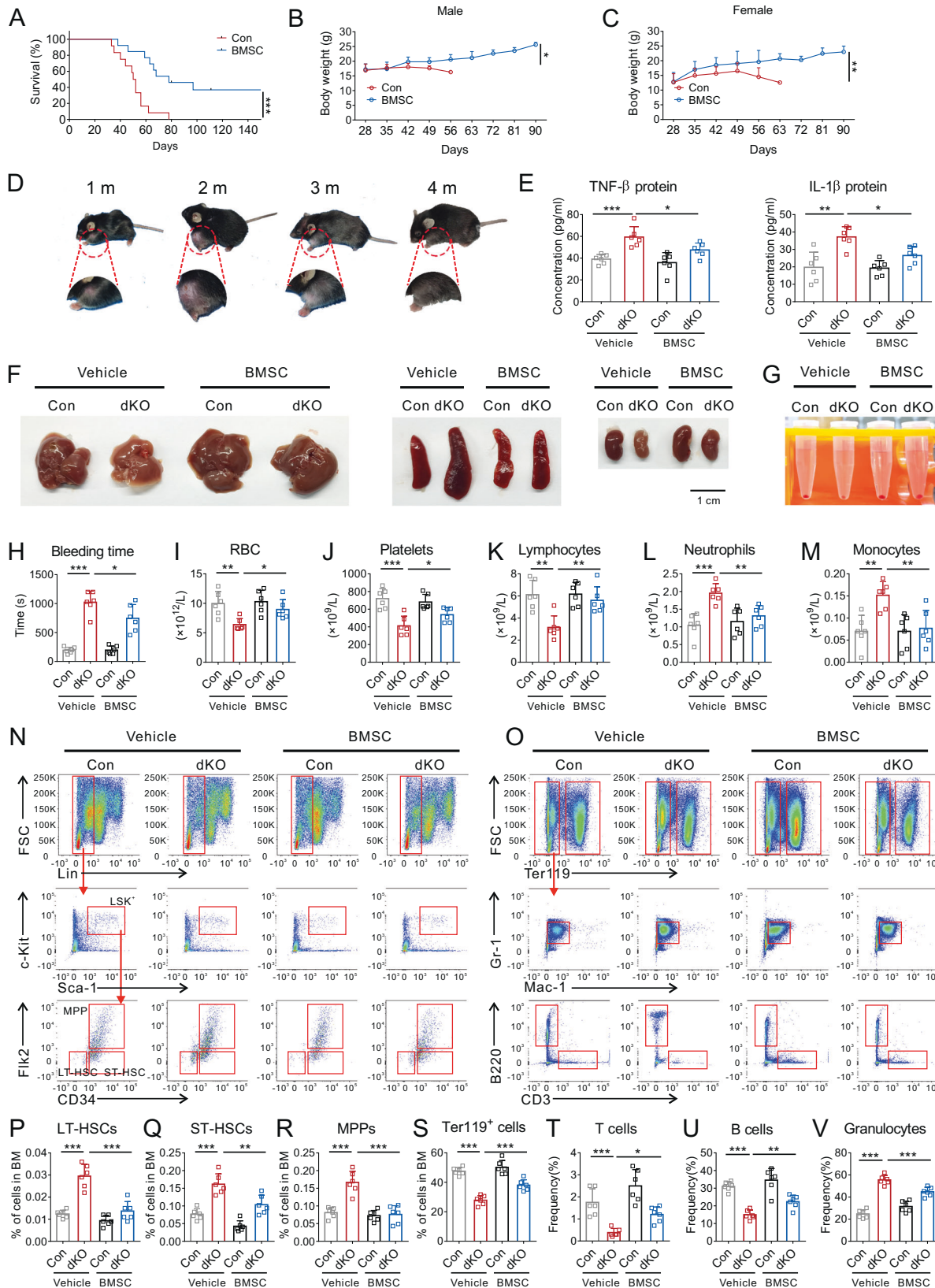
least one unique peptide was filtered for analysis. Overview of protein identification through database retrieval was shown in Fig. S10C. A total of 729 and 1022 differentially expressed proteins with at least a 1.5-fold change were identified in bone marrow cells and supernatants, respectively (Fig. S10D, E). Interestingly, we found a high-abundant protein around 65 kDa in the bone marrow supernatant samples, which was decreased in dKO group (Fig. S10A, B). Based on the results of LC-MS/MS, we identified it albumin,

Fig. 4 **Intravenous injection of BMSCs ameliorates immune and hematopoietic function of dKO mice. A** Survival curves of mice after treatment of BMSCs (10^6 BMSCs dissolved in normal saline per mouse, $n = 12$). **B, C** Body weight change of mice after treatment of BMSCs ($n = 6$–12 at each time point). **D** Representative pictures of 1 to 4-month-old male control and dKO mice subjected to BMSCs. **E** Serum TNF-α and IL-1β concentrations in male control and dKO mice 2 months after subjected to BMSCs or 1 month after subjected to corresponding vehicle ($n = 6$). **F** Representative pictures of organs from male control and dKO mice subjected to BMSCs or corresponding vehicle. **G** Whole bone marrow cells of the tibia or femur from male control and dKO mice subjected to BMSCs or corresponding vehicle. **H** Tail bleeding time measured in male control and dKO mice subjected to BMSCs or corresponding vehicle ($n = 6$). **I–M** Routine blood examination of male control and dKO mice subjected to BMSCs or corresponding vehicle ($n = 6$). **N–V** FACS analysis of bone marrow cells in male control and dKO mice subjected to BMSCs or corresponding vehicle ($n = 6$). Data are mean ± SD of 3 independent experiments. *$P < 0.05$; **$P < 0.01$; ***$P < 0.001$.

suggesting that Pinch loss weakened the liver function. We performed Gene Ontology (GO) enrichment analysis and Kyoto Encyclopedia of Genes and Genomes (KEGG) pathway enrichment analysis of these proteins. In the biological process classification of GO analysis, we noticed that regulation of monocyte chemotaxis and nitric-oxide synthase activity was significantly changed in dKO bone marrow cells (Fig. S11A). In addition, blood coagulation, fibrin clot formation, acute-phase response, acute inflammatory response and immune response were dramatically altered in dKO bone marrow supernatants (Fig. S11B). In the KEGG enrichment analysis, we found that nitrogen metabolism, Toll-like receptor signaling, inflammatory mediator regulation of TRP channels were significantly changed in bone marrow cells from dKO mice (Fig. S11C). Meanwhile, complement and coagulation cascades and staphylococcus aureus infection were significantly changed in bone marrow supernatants from dKO mice (Fig. S11D). Then we classified the function of differentially expressed proteins according to human diseases (Fig. S11E, F). Interestingly, these proteins were highly correlated to infectious diseases and immune diseases. Through combining the analyses of three infectious diseases datasets or two datasets (infection disease versus immune disease), we found some common altered proteins (Fig. 5A, B). The complement lectin cascades were most significantly changed with most enriched protein numbers (Fig. 5C). Moreover, the proportion of Lepr$^+$ BMSCs regulating complement activation was dramatically decreased in dKO versus control mice (Fig. 1E, G, J) Thus, we next focused our studies on the complement pathway.

The complement pathway consists of classical, alternative, and lectin pathways, which plays a vital role in defending invading microorganisms, such as bacteria, fungi, viruses, and parasites. According to our LC-MS/MS results, the levels of Mbl2 (mannose-binding lectin 2), a C-type serum lectin, were significantly reduced both in the bone marrow (Fig. 5D) and serum (Fig. 5E) in dKO mice compared to those in control mice. We also detected some other downstream complement components, including C2, C5, C8b and C9, by ELISA (Fig. 5F, G) or qPCR analyses (Fig. 5H, I), which showed a decreasing trend in cKO relative to control mice. Saa2 is an acute-phase protein produced by liver cells and secreted into the serum, which is a sensitive indicator for diagnosing viral and bacterial infections. The results in the proteomics showed that Saa2 was markedly increased in the dKO mice, which was validated in the qPCR experiments (Fig. 5I).

Since Mbl2 is primarily produced by the liver into the circulation to respond as an acute-phase reactant, we next examined the histological change of the liver tissue in dKO mice. As shown in Fig. 5J, the hepatic lobule architecture in the dKO group was blurred and hepatic sinusoid argyrophilic fiber was hard to be observed. Moreover, TUNEL$^+$ cells, F4/80$^+$ cells, and α-SMA$^+$ cells were remarkably increased in the liver tissue of the dKO versus control mice (Fig. 5J–M), suggesting enhanced apoptosis, inflammatory macrophage infiltration, and fibrosis in the liver of dKO mice. We examined expression levels of markers of macrophage M1- or M2-like polarization by qPCR analyses. However, we did not find a significant alteration of macrophage polarization in dKO mice (Fig. S11G, H). Results from western blotting showed that the level of Mbl2 protein was dramatically reduced in cKO versus control livers in the liver (Fig. 5N, O).

### BMSC-derived Cxcl12 activates Mbl2 expression in hepatocytes

To further investigate the mechanism of Pinch regulating Mbl2 production, we performed co-culture experiments through the transwell system. Primary hepatocytes were cultured in the lower layer and either normal BMSCs or dKO BMSCs were cultured in the upper layer for 48 h. As shown in Fig. 5P, Q, Mbl2 protein level was significantly elevated in primary hepatocytes co-cultured with wild-type BMSCs but not dKO BMSCs. This suggested that BMSCs might regulate the Mbl2 expression via secreting soluble factors and Pinch plays a critical role in regulating the secretome of BMSCs. Cxcl12 in the bone marrow controls the hematopoietic cell trafficking and adhesion during many pathological processes, including heart failure, inflammation and autoimmune diseases [15, 16]. A number of studies demonstrated that Cxcl12 secreted by MSCs plays a notable role in stimulating oval cells, leading to liver cell regeneration [31, 32]. Oval cells, demarcated as precursor cells within the liver, are highly relevant in the field of regenerative medicine [33]. Combining the single-cell RNA sequence data and proteomics data, we found that the expression and secretion of Cxcl12 was decreased in mice lacking Pinch in BMSCs, which was further validated by ELISA assay (Fig. 5R). Then, we examined whether Cxcl12 could affect the expression of Mbl2 in the hepatocytes. Primary hepatocytes were treated with recombinant mouse Cxcl12 for 24 h, followed by western blotting. Results showed that Cxcl12 dramatically increased the level of Mbl2 protein in primary hepatocytes in a dose-dependent manner (Fig. 5S, T).

Recombinant mouse Mbl2 protein reduces the lethality of dKO mice

We next administrated various dosages of recombinant mouse Mbl2 protein into dKO mice intravenously twice a week for 2 weeks (Fig. 5U). We found that Mbl2 significantly prolonged the lifespan of the dKO mice without dosage dependent (in the range of 10–100 µg/kg body weight) (Fig. S11I). Thus, we continued to investigate whether Mbl2 could elevate the survival rate further with extra doses. We administrated 10 µg/kg of recombinant mouse Mbl2 into dKO mice intravenously twice a week for 4 weeks (Fig. 5V). Strikingly, around 50% of mice could survive until 90 days (Fig. 5V). Afterwards, we examined the peripheral concentration of Mbl2 by ELISA. Either administration of BMSCs or rm-Mbl2 could elevate the Mbl2 level in blood to maintain the homeostasis of innate immune system (Fig. S11J).

Pinch deficiency largely reduces the ability of BMSCs to suppress LPS-induced acute lung injury in mice

To further investigate the immunoregulatory role of Pinch in stromal cells, we established the lipopolysaccharide (LPS)-induced acute lung injury (ALI) mouse model, a well-accepted model for investigating sepsis because it mimics pathological events such as the inflammatory and histological changes observed in this disease. To examine the spontaneous movement and exploratory behavior of ALI mice, an open field experiment was conducted. We isolated and cultured BMSCs from Pinch2$^{-/-}$ mice and then depleted Pinch1 using Pinch1 siRNA to harvest BMSCs lacking Pinch1/2 (referred to as BMSC^{dKO} hereafter). Initially, mice were given vehicle or BMSC or BMSC^{dKO} with the LPS challenge
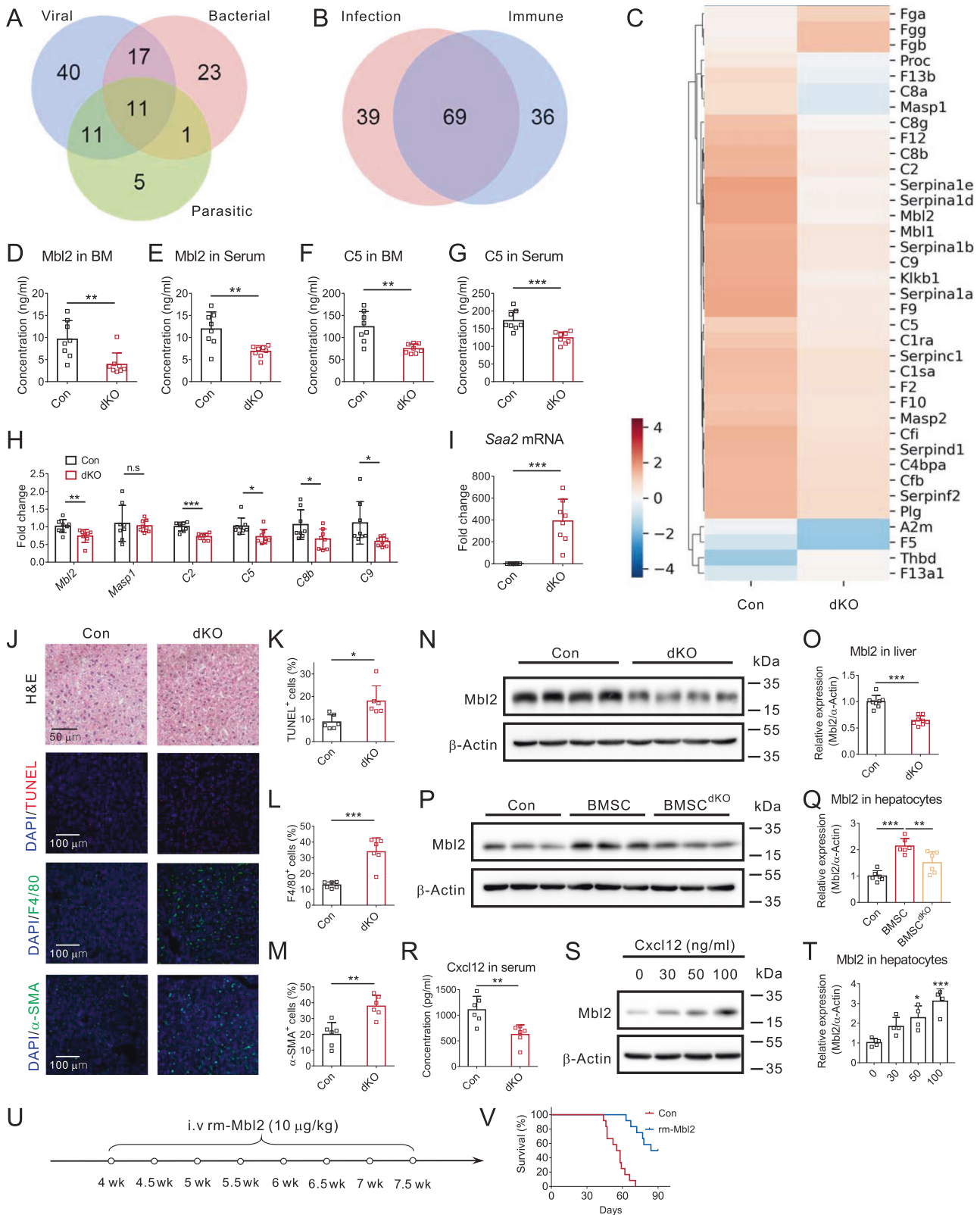
simultaneously. Lipopolysaccharide (LPS) serves as the outer membrane constituent of gram-negative bacteria, which plays a crucial role as the primary causative agent in the development ALI by instigating an inflammatory response. The open field experiment was carried out to explore the spontaneous movement and exploratory behavior of ALI mice (Fig. 6A–F). Administration of BMSCs markedly reversed the LPS-induced downregulation of total distance covered (Fig. 6B), movement time (Fig. 6C), time in the center zone (Fig. 6D), distance in the center zone (Fig. 6E), and line crossing frequencies (Fig. 6F). In contrast, BMSC[dKO] did not

Fig. 5 Complement lectin pathway contributes to hematopoietic and immune-regulatory roles of Pinch1/2. A Venn diagram of dysregulated factors related to infectious diseases in the bone marrow supernatant of dKO mice. **B** Venn diagram of dysregulated factors in the bone marrow supernatant of dKO mice (infectious disease or immune disease). **C** Heatmap of dysregulated factors in the complement and coagulation cascades identified through MS in the bone marrow supernatant from control mice and dKO mice. The level of Mbl2 in bone marrow supernatant (**D**) or serum (**E**) from control mice and dKO mice ($n = 8$). The level of Complement component 5 in bone marrow supernatant (**F**) or serum (**G**) from control mice and dKO mice ($n = 8$). **H, I** qPCR analysis of some dysregulated factors in the complement and coagulation cascades identified through MS in the bone marrow supernatant from control mice and dKO mice ($n = 8$). **J** Representative images of H&E staining, TUNEL staining, and IF staining of F4/80 and α-SMA. Quantification of TUNEL$^+$ cells (**K**), F4/80$^+$ cells (**L**) and α-SMA$^+$ cells (**M**) in the liver ($n = 6$). Data are mean ± SD of 3 independent experiments. **N, O** Representative protein expression level ($n = 8$ in total) and quantification of Mbl2 in the liver ($n = 8$ in total). Data are mean ± SD of 3 independent experiments. **P, Q** Representative protein expression level ($n = 6$ in total) and quantification of Mbl2 in primary hepatocytes co-cultured with BMSC or BMSC^{dKO}. Data are mean ± SD of 3 independent experiments. **R** The level of Cxcl12 in serum from control mice and dKO mice ($n = 6$). **S, T** Representative protein expression level and quantification of Mbl2 in primary hepatocytes stimulated with Cxcl12 for 24 h ($n = 4$). Data are mean ± SD of 3 independent experiments. **U** A schematic diagram illustrating the experimental design of rm-Mbl2 administration. **V** Survival curves of mice after treatment rm-Mbl2 (dissolved in normal saline, $n = 12$). *$P < 0.05$; **$P < 0.01$; ***$P < 0.001$.

exert such effects. Furthermore, BMSCs reduced mortality of mice challenged with a higher LPS dose while deleting Pinch abolished the effect (Fig. 6G). Mice subjected to LPS revealed marked impairment of lungs 24 h after LPS injection. The histology was determined by H&E staining in lungs from the mice (Fig. 6H) followed by lung injury scores (Fig. 6I). Compared with the findings of the control group, the pathological features of the lungs in the LPS group were as follows: edema, alveolar wall thickening, alveolar congestion, and hemorrhage. Compared to LPS alone, the administration of BMSCs alleviated the histopathologic characteristics while BMSC^{dKO} was not as effective as BMSCs. Additionally, we evaluated the TNF-α level in the serum after LPS challenge, which is mainly responsible for pro-inflammatory signals on LPS-induced inflammation. BMSC treatment dramatically inhibited the secretion of TNF-α into the circulation, while the anti-inflammatory role of BMSC^{dKO} was much weaker (Fig. 6J).

Pinch loss greatly impairs BMSC suppression of DSS-induced inflammatory bowel disease in mice
Inflammatory bowel disease, including both Crohn's disease and ulcerative colitis (UC), is a chronic multifactorial disease which affects the gastrointestinal tract and probably correlates to an aberrant immune response [34]. MSCs have shown effectiveness in the treatment of UC through MSC transplantation [35], [36]. We constructed dextran sodium sulfate (DSS)-induced UC model to further verify the immunoregulatory role of Pinch in vivo. Mice subjected to DSS showed significant decreased colon length (Fig. 7A and B), weight loss (Fig. 7C) and an increase in disease activity scores (DAI) (Fig. 7D). These effects were reversed by BMSCs, as reflected by increased colon length and the decline in weight loss percentage and DAI compared to those exhibited by UC. On the contrary, BMSC^{dKO} did not show such effects. Histological scoring revealed that BMSCs attenuated the structural destruction of colon tissue, inhibited inflammatory cell infiltration, and crypt loss (Fig. 7E, F). Nevertheless, the effects of BMSC^{dKO} against colitis were limited. In DSS-induced UC, the survival rate of mice treated with BMSCs (UC + BMSC group) was significantly higher than those treated with PBS (UC group) or BMSC^{dKO} (UC+BMSC^{dKO} group), indicating that Pinch exerts a critical role in the relief of UC symptoms (Fig. 7G).

DISCUSSION
In this study, we demonstrate an important interaction between bone and liver to maintain immune and hematopoietic function. Specifically, we find that Pinch proteins maintain normal immune function and hematopoiesis by promoting Cxcl12 expression in BMSCs, which stimulates production of Mbl2 in hepatocytes. Thus, Pinch loss in Prx1$^+$ cells reduces activation of the lectin complement pathway and increases susceptibility to infection. The novel Pinch-Cxcl12-Mbl2 signaling modulates both immunity and hematopoiesis to maintain the body homeostasis. Our

findings may provide a therapeutic strategy for infectious and immune diseases, such as sepsis and inflammatory bowel disease.

Pinch, a FA protein, functions as an adapter to form multi-protein complexes that connect different signaling pathways. Our study reveals that Pinch signaling in BMSCs controls the expression of Mbl2 in hepatocytes. Pinch loss in Prx1$^+$ cells impairs the complement lectin pathway, which is one of the most significantly altered pathways in Pinch mutant mice. Recent studies indicate that MBL plays a crucial role in the complement lectin pathway and the innate immune system. MBL deficiency is common and renders individuals more susceptible to numerous infectious diseases [37, 38]. Research on coronaviruses has shown that MBL may be a promising target for preventing SARS-CoV-2 infection, particularly in individuals with genetically determined low levels of serum MBL, which increases the risk of cytokine storms and susceptibility to SARS-CoV-2 [39]. Clinical studies have investigated the use of plasma-derived or recombinant material to supplement low MBL levels (reviewed in [25]). We find that consecutive supplement of rm-Mbl2 can reduce the occurrence of infection in Pinch mutant mice and inhibit excessive inflammatory responses, subsequently prolonging their lifespan. Our research may improve our understanding of the complex mechanism of skeletal stem and progenitor cells in regulating complement activation in the liver and provide new insights for future MSC-based therapeutic agents.

MSCs have been studied in numerous clinical trials for their immunomodulatory capacity in various medical conditions [40–42]. MSCs can obstruct inflammatory processes and generate regulatory cells, primarily through the secretion of soluble factors [43]. The development of BMSC-BMM and BMSC-macrophage co-cultures has substantially contributed to our understanding of MSC Pinch-mediated regulation of inflammation through its paracrine effects. Manipulating the functions of endogenous MSCs for therapeutic use may therefore be an attractive alternative to current treatment modalities for inflammatory conditions. BMSC-derived Cxcl12 promotes an IL-10$^+$-macro-phage-amplified anti-inflammatory response in toxic colitis [44]. An association of the functional impairment of Pinch signaling and reduction in Cxcl12 expression is noted by us based on scRNA-seq and proteomics analyses, emphasizing the important role of the bone marrow-derived chemokines regulating the innate immune function in the liver. Therefore, targeted upregulation of the Cxcl12-Mbl2 axis could potentially provide support for the remaining normal hematopoiesis, thereby augmenting the abilities of normal hematopoietic progenitors. According to our experimental data from this study, administration of BMSCs has a significant therapeutic effect on associated complications and sickness behaviors in Pinch mutant mice, elevating the survival rate via the anti-inflammatory and immunoregulatory functions. However, some of the dKO mice treated with BMSCs or rm-Mbl2 still cannot survive for more than 4 months. Dose and
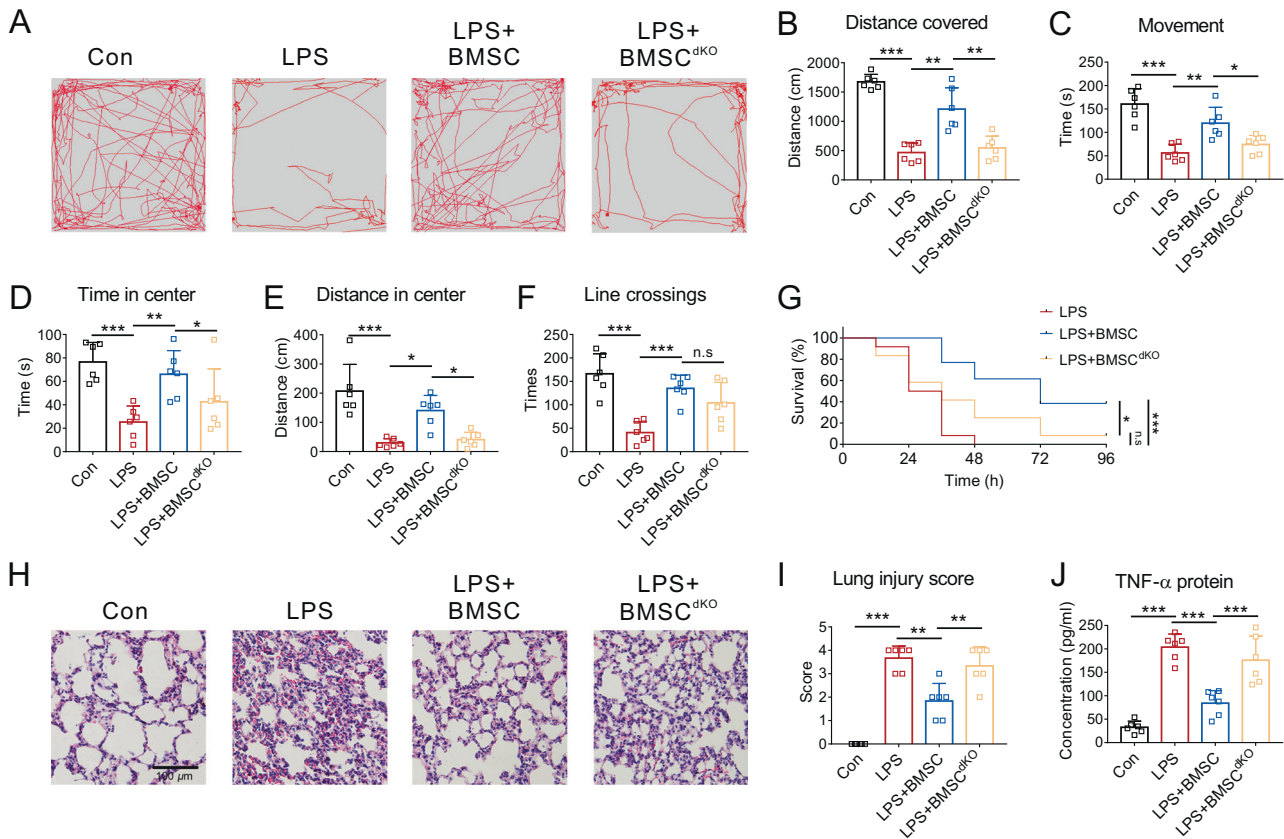
Fig. 6 Depletion of Pinch impairs the effects of BMSCs in treatment of acute lung injury induced by LPS. A–F Track plots (**A**), distance covered (**B**), movement time (**C**), distance covered in the center zone (**E**), and line crossing times (**F**) during the open field test. Mice were administrated with BMSC or BMSC^{dKO} or corresponding vehicle (normal saline) followed by administration of LPS (10 mg/kg) or normal saline ($n = 6$). **G** Survival curve of LPS-induced acute lung injury. Mice were administrated with BMSC or BMSC^{dKO} or corresponding vehicle (normal saline) followed by administration of LPS (30 mg/kg) or normal saline ($n = 12$). **H, I** Representative images of H&E staining for lung sections 24 h after acute lung injury model followed by quantification (scale bar = 100 μm). **J** Serum TNF-α concentrations in mice 24 h after administrated with BMSC or BMSC^{dKO} followed by administration of LPS ($n = 6$) Results were normalized to Gapdh. Data are mean ± SD of 3 independent experiments. *$P < 0.05$; **$P < 0.01$; ***$P < 0.001$.
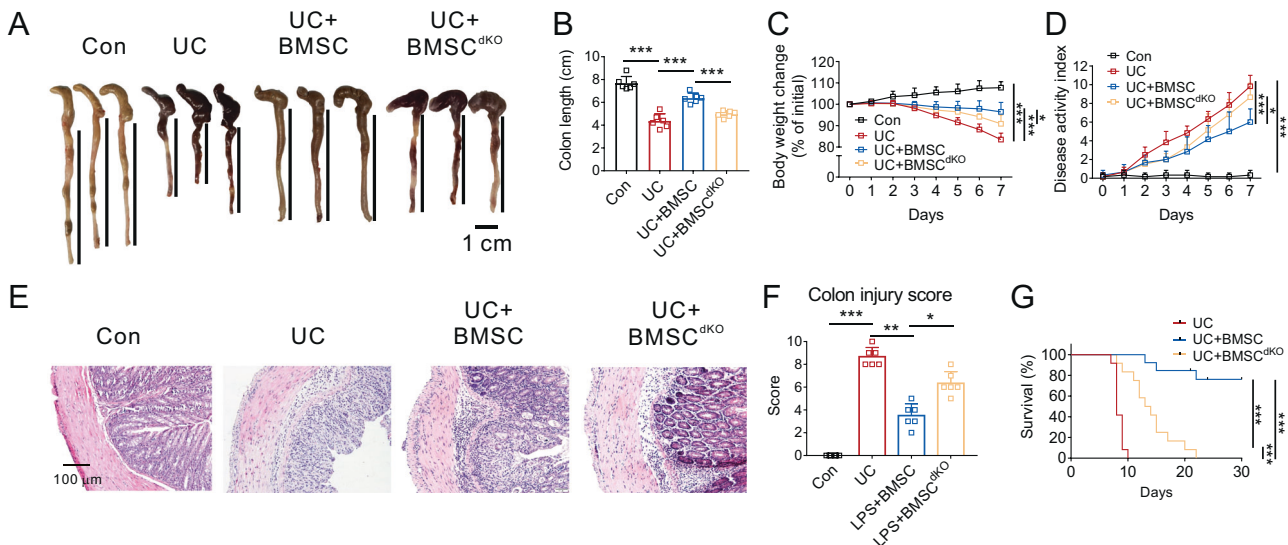
Fig. 7 Depletion of Pinch impairs the effects of BMSCs in treatment of DSS-induced experimental colitis in mice. A Macroscopic appearances of colons in each group mice. **B** The quantification of colon length ($n = 6$). **C** Loss of basal body weight from day 0 to day 7 (%) after DSS induction ($n = 6$). **D** Mean DAI evaluations from day 0 to day 7 in each group ($n = 6$). **E, F** H&E staining of colonic sections (scale bar = 100 μm) followed by quantification. **G** Survival curve of DSS-induced acute inflammatory bowel disease. Mice were administrated with BMSC or BMSC^{dKO} or corresponding vehicle (normal saline) followed by freely drinking water containing DSS (4%) or normal drinking water for 7 days ($n = 12$). Data are mean ± SD of 3 independent experiments. *$P < 0.05$; **$P < 0.01$; ***$P < 0.001$.

administration routes might contribute to the highly variable outcomes of MSC treatment. In addition, other mechanisms besides Cxcl12-Mbl2 might contribute to immunomodulatory capacity of MSCs. Based on promising data, we also examine the efficacy of BMSCs in addressing critical illnesses, such as sepsis and inflammatory bowel diseases, which have exhibited potential effectiveness in MSC-based therapies [45]. Our results are consistent with previous reports that BMSCs have potential for treating sepsis and inflammatory bowel disease, while we firstly find that the loss of Pinch proteins largely abolishes the therapeutic effects of BMSCs. Our results provide new insights into the mechanisms underlying the effects of MSC treatment.

Our results from single-cell RNA-seq analyses demonstrate that Pinch signaling in Prx1$^+$ cells plays a pivotal role in maintaining the normal cell subpopulations in the bone marrow. Logan et al. [46] reported that Prx1 is highly expressed by limb bud and head mesenchymal progenitors. Through genetic lineage tracing by Prx1-Cre, Prx1 was found to be able to label all skeletal lineage cells, including skeletal stem and progenitor cells, osteoblasts, osteocytes, chondrocytes, and adipocytes. Recently, Liu and co-workers [47] found that besides stem cells in skeletal system, Prx1 could also mark stem cells in white adipose tissue and dermis in mice despite sharing some distinct other markers in different tissue. These observations still need to be varified by other investigators. According to our scRNA-seq results, Prx1$^+$ cells are highly overlapped with Pinch1$^+$ cells (around 67%) in the bone marrow. Lepr$^+$ BMSCs highly express Pinch1 (around 68%). That is, Pinch ablation in Prx1$^+$ cells mainly affected Lepr$^+$ BMSCs in the bone marrow. Pinch loss in Prx1$^+$ cells causes proportional and functional changes of multiple bone marrow cells. Our subsequent functional verification experiments could also explain, at least in part, that Pinch in BMSCs is vital in exerting their anti-inflammation, immune regulation and hematopoietic regulation properties. Strikingly, four BMSC clusters are differently distributed in control mice and mutant mice and Pinch loss significantly reduces the numbers of BMSCs. BMSCs are mostly in cluster 2 and 15 in mutant mice, which are highly associated with inflammatory and immune responses. The cell count of cluster 1, which is responsible for complement activation, is dramatically reduced in mutant mice. This is consistent to our LC-MS/MS results that Mbl2-mediated complement lectin pathway is impaired in mutant mice, we considered which is the major reason of the premature death of the mutant mice. The present discourse concerns the role of pericytes, which are a type of microvascular mural cells that possess direct contact with endothelial cells, in the host response to injuries. The proportion and the subpopulation of pericytes and endothelial cells are markedly changed due to the Pinch loss, indicating that Pinch proteins are functionally important components in the bone marrow niche in mice to maintain homeostatic conditions during development. Moreover, the subpopulation of osteoprogenitors, osteoblasts, and chondrocytes are dramatically changed, which may in part explain our previous results that Pinch loss impairs both chondrogenesis and osteogenesis in mice [22].

In the present study, we demonstrate the importance of the Pinch signaling in control of hematopoiesis. While it is known that MSCs can control the production of various blood cells over the course of one's life through a process commonly termed hematopoiesis [48], the underlying mechanisms are still incompletely understood. The main traits that distinguish HSCs are self-renewal and differentiation capabilities, which span across all hematopoietic blood lineages. Furthermore, niches in the bone marrow serve as the principal microenvironments that harbor and maintain hematopoietic stem and progenitor cells. MSCs, in turn, play a critical role in constituting proper niches for these blood cells in both adult and developing bone marrow, thereby regulating hematopoietic homeostasis and enabling the hematopoietic system's response to stress conditions [49]. In this study, we find that Pinch signaling from Prx1$^+$ cells impacts multiple aspects of the hematopoiesis in mice. Pinch loss in Prx1$^+$ cells stimulates the differentiation to neutrophils, monocytes and granulocytes and, in the meantime, inhibits the differentiation to RBCs, platelets and lymphocytes.

Several limitations of this study should be noted. First, our study suggested that Cxcl12 secreted by BMSCs plays a key role in the regulation of Mbl2 synthesis and activation of complement lectin pathway to relive sickness behaviors of Pinch mutant mice. However, how Cxcl12 activates Mbl2 expression remains unknown. Second, the long-term effects of BMSC treatment have not been established in this study. Whether extra doses of BMSCs will further promote the therapeutic effects or any long-term risks of BMSC treatment are currently unknown. Third, the implementation of such knowledge in MSC clinical settings necessitates the development of methods that offer a detailed examination of the intricate immune constituents and effector molecules in inflamed tissue microenvironments associated with distinct disease phenotypes.

In conclusion, our data provide the first evidence that BMSC Pinch signaling is vital in maintaining hematopoiesis and immune balance by regulating the complement lectin pathway. Mice lacking Pinch proteins in Prx1$^+$ cells can be rescued by supplementation of normal BMSCs or rm-Mbl2. In the absence of Pinch signaling, the protective effects of BMSCs against inflammation are significantly weakened. The effects of BMSCs on hematopoiesis maintenance and immune regulation might be partially mediated by Cxcl12-Mbl2 axis. The present study has revealed a distinct mechanism of therapeutic interventions using BMSCs, thereby providing valuable insights for the improved utilization of BMSCs to mitigate the occurrences of infectious and immune-mediated disorders.

METHODS

Animal studies

To minimize the possibility that incomplete Cre mediated excision would occur in the case of four floxed alleles of Pinch1 and Pinch2, we generated a compound Pinch1 and Pinch2 double knockout mouse line with mesenchymal progenitors specific Pinch1 knockout alleles and Pinch2 null alleles. Prx1-Cre; Pinch1$^{f/f}$; Pinch2$^{-/-}$ transgenic mice were generated in our lab as described previously [22]. Pinch1$^{f/f}$ mice were first crossed with Pinch2$^{-/-}$ mice to generate Pinch1$^{+/+}$; Pinch2$^{+/-}$ mice. Pinch1$^{+/+}$; Pinch2$^{+/-}$ mice were then crossed to each other and generate the Pinch1$^{f/f}$; Pinch2$^{-/-}$ mice. Male Prx1-Cre mice were crossed with female Pinch1$^{f/f}$; Pinch2$^{-/-}$ mice to generate Prx1-Cre; Pinch1$^{f/+}$; Pinch2$^{+/-}$ mice. Finally, male Prx1-Cre; Pinch1$^{f/+}$; Pinch2$^{+/-}$ mice were bred with female Pinch1$^{f/f}$; Pinch2$^{-/-}$ mice to generate Prx1-Cre; Pinch1$^{f/f}$; Pinch2$^{-/-}$ mice, which are double knockout mice. Experimental mice were weaned at day of postnatal 21, with 1 mm of tail tissue collected. Mouse genome DNAs were extracted from tail tissue with Mouse Direct PCR Kit (B40013, Bimake, Houston, TX, USA) following the manufacturer's protocol. PCR and agar gel examination were performed for mouse genotyping and sequences of primers are listed in Supplementary Table 1. Mice used in this study, including Prx1-Cre, Pinch1$^{f/f}$ and Pinch2$^{-/-}$ mice, have been maintained in our laboratory by breeding with normal C57BL/6 mice for over 10 generations. C57BL/6 mice were purchased from the Vital River Laboratory Animal Technology Company (Beijing, China). All animal experiments were conducted in the specific pathogen free (SPF) Experimental Animal Center of Southern University of Science and Technology. Animals were housed 4/cage at 20–24 °C, exposed to a 12 h/12 h light/dark cycle, and given water and rodent chow ad libitum. Mice were monitored daily. All protocols for animal use were approved by the Institutional Animal Care and Use Committee (IACUC) at the Southern University of Science and Technology. The group allocation and results analysis in this study were conducted by the investigators in a blinded manner.

Cell culture and transfection

RAW264.7 cells were purchased from Wuhan Sunncell Biotechnology Co., Ltd (SNL-112, Wuhan, China), which were originated from American Type Culture Collection, USA. RAW264.7 with less than 10 passage numbers were used. Cell lines were authenticated by short tandem repeat profiling

using the genetic analyzer (3730XL, Applied Biosystems, USA) and tested for mycoplasma contamination using MycoBlue Mycoplasma Detector (Vazyme, Nanjing, China). Cells were grown in DMEM supplemented with 10% (v/v) fetal bovine serum (FBS).

Isolation of primary bone marrow stromal cells (BMSCs) was performed as we previously described [50]. In brief, limb bones of the mice were isolated, and bone marrow cells were flushed with α-minimum Eagle's medium containing 20% FBS and 1% penicillin/streptomycin into a 100-mm dish. Non-adherent cells were removed 48 h later, and the adherent cells were cultured and passaged in the same medium for 8–10 days. The MSCs were characterized by the expression of surface phenotypic markers as described previously using flow cytometry [51]. Between third and fifth generation, BMSCs were used for experiments. To obtain Pinch1/2^{dKO} BMSCs, we transfected a Pinch1 siRNA (20 nM) as well as the corresponding negative controls into BMSCs from Pinch2$^{-/-}$ mice for 48 h using Lipofectamine 3000 (Invitrogen, Carlsbad, USA) according to the manufacturer's instructions. The siRNA sequence was listed in Supplementary Table 2. The efficiency of knockdown was measured via real-time PCR and western blotting.

Flow cytometry
Single cell suspensions of bone marrow cells were prepared at a concentration of 1×10^7 cells per ml in PBS plus 0.1% BSA. Cells were blocked with 2% Fc Receptor block (eBioscience) in PBS for 15 min on ice. The antibody information is shown in Supplementary Table 3. Flow cytometry analysis was performed with a FACSCanto instrument (BD Biosciences). The flow cytometry data were analyzed using FlowJo 3.3 software (Tree Star, San Carlos, CA, USA).

Histology and immunohistochemistry
After fixation in 10% normal saline for 24 h, lung and colon tissues were washed under tap water and then serial dilutions of ethanol were used for dehydration. Specimens were cleared in xylene and embedded in paraffin. Paraffin bees wax tissue blocks were prepared for sectioning at 5-μm thickness by slide microtome. The obtained tissue sections were collected on glass slides, deparaffinized, rehydrated, and stained by hematoxylin and eosin (H&E) stain or TUNEL stain for examination under the microscope (Olympus BX53). Histological microscopic assessment was performed in a blinded fashion by the same person. A scoring system of lung injury scores was assigned graded from 0 = minimal (little) damage, 1+ = mild damage, 2+ = moderate damage, 3+ = severe damage, and 4+ = maximal damage [52]. A scale for evaluating colon tissue sections was according to the severity of inflammation (0, none; 1, mild; 2, moderate; 3, severe), extent of inflammation (0, none; 1, mucosa; 2, mucosa and submucosa; 3, transmural), and crypt damage (0, none; 1, basal one-third damaged; 2, basal two-thirds damaged; 3, crypt lost but surface epithelium present; 4, crypt and surface epithelium lost) [53]. The final score was the sum of the scoring, and the possible maximum score was 10.

Paraffin-embedded tissue sections were dewaxed, rehydrated, and subjected to antigen retrieval before permeabilization. Thereafter, the sections were washed with 0.3% TritonX-100 in PBS and blocked with 1% BSA in 0.3% TritonX-100/PBS for 1 h at room temperature, and then incubated overnight with primary antibodies diluted in 1% BSA in 0.3% TritonX-100/PBS at 4 °C, and washed three times with PBS. Then, the samples were incubated with the appropriate secondary antibody for 2 h at room temperature. The antibody information is shown in Supplementary Table 3. To visualize the cell nuclei, sections were counterstained with DAPI for 10 min at room temperature. The stained sections were examined using a fluorescence microscope (LSM 980, Zeiss, Oberkochen, Germany).

Enzyme-linked immunosorbent assay (ELISA)
Mouse TNF-α ELISA kit (EK0527, BOSTER Biological Technology, Pleasanton, CA, USA), Mouse IL-1β ELISA kit (EK0394, BOSTER Biological Technology, Pleasanton, CA, USA), Mouse Mbl2 ELISA Kit (EK0806, BOSTER Biological Technology, Pleasanton, CA, USA), and Mouse Complement C5a ELISA Kit (EK0987, BOSTER Biological Technology, Pleasanton, CA, USA) were used to detect the concentrations of proteins in the cell culture media or serum according to the manufacturer's instructions.

Lipopolysaccharide (LPS)-induced acute lung injury model in mice
Male C57BL/6 mice (6–8 weeks of age, 25–30 g) were randomly divided into 4 groups (18 mice per group, which were sufficient to obtain statistical differences) and injected intravenously with vehicle (normal saline), BMSC (10^6 BMSCs per mouse from Pinch2$^{-/-}$ mouse, dissolved in 0.1 ml normal saline), or BMSC^{dKO} (10^6 Pinch1/2^{dKO} BMSCs per mouse, dissolved in 0.1 ml normal saline). Simultaneously, the mice were intraperitoneally injected with 10 mg/kg (30 mg/kg for survival experiment) LPS (L4524, Sigma-Aldrich, USA) or normal saline. Open field test was utilized to determine locomotor activity after mice were subjected to LPS for 3 h as previously described [54]. Mice were gently placed into the center of the open field box (ZS Dichuang, Beijing, China) and the total distance traveled and time spent in the inner and outer zones were measured for 5 min. These were recorded by an overhead camera and analyzed with TopScan software (Any-maze™, Stoelting Co.). Total distance, movement time/distance, line crossings, time/distance in the central zone were recorded and analyzed. After 24 h, the mice were anesthetized with 5% isoflurane. Serum was collected, and bronchoalveolar lavage was performed and the mice were intracardially perfused with normal saline. The whole lung was carefully removed for the following study.

Dextran sulfate sodium salt (DSS)-induced ulcerative colitis (UC) model in mice
Male C57BL/6 mice (6–8 weeks of age, 25–30 g) were randomly divided into 4 groups (18 mice per group, which were sufficient to obtain statistical differences): control, UC, UC + BMSC treatment, and UC + BMSC^{dKO} treatment. To induce UC, the mice were exposed to 4% DSS (42867, Sigma-Aldrich, USA) in the drinking water for seven days. BMSC or BMSC^{dKO} treatment was performed via intravenous injection of 10^6 cells dissolved in 0.1 ml normal saline per mouse on Day 0 and Day 3. Non-treated mice were injected with the same amount of normal saline. During the duration of the experiment, a disease activity index (DAI) score was assessed to evaluate the clinical progression of colitis according to weight loss: 0 (no loss), 1 (1–5%), 2 (5–10%), 3 (10–20%), and 4 (>20%); stool consistency: 0 (normal), 2 (loose stool), and 4 (diarrhea); and bleeding: 0 (no blood), 1 (Hemoccult positive), 2 (Hemoccult positive and visual pellet bleeding), and 4 (gross bleeding, blood around anus) [55]. The final clinical score was the sum of the scoring, and the possible maximum score was 12. All mice were sacrificed seven days after treatment to obtain blood and colon tissue samples. The colons were subjected to macroscopic assessment and further processed for microscopic histological evaluation and molecular detection.

Real-time quantitative polymerase chain reaction
One microgram of RNA was reverse transcribed with the HiScriptQ RT SuperMix for qPCR (Vazyme, Nanjing, China). cDNA was analyzed by qPCR using the SYBR qPCR Master Mix (High ROX Premixed, Vazyme), a CFX384 real-time System C1000 Thermal Cycler (Bio-Rad) and the Bio-Rad CFX Manager 3.1 software. The reaction conditions were as follows: 95 °C for 10 min followed by 40 cycles of 95 °C for 10 s and 60 °C for 1 min. The relative amount of the different mRNAs was quantified with the ΔΔCt method with Gapdh as normalization. The information of the primers is described in Supplementary Table 4.

Single-cell RNA sequencing and analysis
Equivalent cells from three mice were pooled together and used for 10X single-cell library construction and further single-cell RNA sequencing analysis. For bone marrow non-adherent hematopoietic cells, two replicates were prepared for control (BM1 Con, BM2 Con) and dKO (BM1 dKO, BM2 dKO) samples. For non-hematopoietic bone marrow cells, hematopoietic cells were pre-depleted using the Lineage Cell Depletion Kit (Miltenyi Biotec, Auburn, USA). Afterwards, Lepr$^+$ cells were sorted out from control and dKO samples by FACS to perform single-cell RNA sequencing based on 10× Genomics Chromium Single Cell 3′ protocol. It is done by partitioning thousands of cells into nanoliter-scale Gel Beads-in-emulsion (GEMs), where all generated cDNA shares a common 10x Barcode. Libraries are generated and sequenced from the cDNA and 10x Barcodes are used to associate individual reads back to the individual partitions. For raw data processing, the Cell Ranger software pipeline (version 5.0.0) provided by 10× Genomics was used to demultiplex cellular barcodes, map reads to the genome and transcriptome using the STAR aligner, and down-sample reads as required to generate normalized aggregate data across samples, producing a matrix of gene counts versus cells. Graph-based clustering was performed to cluster cells according to their gene expression profile using the Find Clusters function. Cells were visualized using a 2-dimensional Uniform Manifold Approximation and Projection (UMAP) algorithm with the Run UMAP function.

Western blot analysis

Protein isolation from whole cerebral cortex or cells was performed as descried previously. The concentration of protein was assessed by BCA assay kit (Thermo Fisher). Western blots were employed using the standard SDS-polyacrylamide gel electrophoresis method and electrotransferred onto PVDF membranes (Millipore, Billerica, MA, USA). After blocking with 5% (w/v) BSA (Solarbio, Beijing, China) in PBS for 2 h, the membranes were incubated with primary antibodies at 4 °C overnight, and then incubated with the corresponding secondary antibody for 1 h at room temperature. At last, the immunoblot was visualized and quantified by a gel densitometric scanning and analysis system (Bio-Rad, Berkeley, CA, USA).

The information of primary antibodies and secondary antibodies were listed in Supplementary Table 3.

Tail bleeding assay

Mice were anesthetized (2.5% Avertin 10 µl/g; i.p.) and placed on a hot plate maintained at 37 °C. Bleeding time assays were performed by cutting off the tip of the tail with a razor blade (5 mm from the tip). The tail was immediately immersed in saline solution heating at 37 °C. The time to stable cessation of bleeding (no rebleeding within 30 s) was visually determined. Bleeding was stopped manually at 20 min, and mice that bled beyond this end point were counted as 20 min.

Blood parameters

Mouse whole blood was collected in anticoagulation tubes containing EDTA. Mouse whole blood cell count was measured using an automatic blood cell analyzer (KX-21, Sysmex Corporation, Kobe, Japan).

Mass spectrometry analysis

Proteomic analysis was performed at the Jingjie PTM BioLab Co. Ltd (Hangzhou, China). Proteomics Facility. Six Pinch1$^{f/f}$; Pinch2$^{-/-}$ mice (Control group) and six Prx1-Cre; Pinch1$^{f/f}$; Pinch2$^{-/-}$ mice (dKO group) were anesthetized with 5% isoflurane. Bone marrow cells and bone marrow supernatants were obtained respectively from the femurs of the mice. After the proteins were extracted and digested, the tryptic peptides were dissolved in solvent A (0.1% formic acid, 2% acetonitrile/in water), directly loaded onto a home-made reversed-phase analytical column (25-cm length, 75/100 µm i.d.). Peptides were separated with a gradient from 6% to 24% solvent B (0.1% formic acid in acetonitrile) over 70 min, 24–35% in 14 min and climbing to 80% in 3 min then holding at 80% for the last 3 min, all at a constant flow rate of 450 nL/min on a nanoElute UHPLC system (Bruker Daltonics). The peptides were subjected to capillary source followed by the timsTOF Pro (Bruker Daltonics) mass spectrometry. The electrospray voltage applied was 1.60 kV. Precursors and fragments were analyzed at the TOF detector, with a MS/MS scan range from 100 to 1700 m/z. The timsTOF Pro was operated in parallel accumulation serial fragmentation (PASEF) mode. Precursors with charge states 0 to 5 were selected for fragmentation, and 10 PASEF-MS/MS scans were acquired per cycle. The dynamic exclusion was set to 30 s. FDR was adjusted to <1%. The resulting MS/MS data were processed using MaxQuant search engine (v.1.6.15.0) embedded into Proteome Discoverer 1.4 software for identification and quantitation analysis. The differentially expressed peptides were subsequently filtered for fold change >1.5.

Statistical analysis

The data in this study are represented as mean ± standard deviation (SD) and calculated using GraphPad Prism 5. Statistical analysis among the frequencies were carried out using non-parametric Manne–Whitney test (Wilcox test), and two-group comparisons were carried out using the unpaired two-tailed Student's t test and multiple groups comparisons were carried out using the One-way ANOVA followed by Bonferroni's test or using the Two-way ANOVA followed by Bonferroni's test. P values lower than 0.05 were considered statistically significant.

DATA AVAILABILITY

All data supporting the findings of this study are available within the article and its Extended Data files or from the corresponding authors upon reasonable request. Source data are provided with this paper. ScRNA-seq data have been deposited in Gene Expression Omnibus under accession No. GSE152217 and LC–MS/MS data have been deposited in PRIDE Archive under accession No. PXD043019.

REFERENCES

1. Singer NG, Caplan AI. Mesenchymal stem cells: mechanisms of inflammation. Annu Rev Pathol. 2011;6:457–78.
2. Uccelli A, Moretta L, Pistoia V. Mesenchymal stem cells in health and disease. Nat Rev Immunol. 2008;8:726–36.
3. Weiss ARR, Dahlke MH. Immunomodulation by Mesenchymal Stem Cells (MSCs): mechanisms of action of living, apoptotic, and dead MSCs. Front Immunol. 2019;10:1191.
4. Weissman IL. Developmental switches in the immune system. Cell. 1994;76:207–18.
5. Gotts JE, Matthay MA. Sepsis: pathophysiology and clinical management. BMJ. 2016;353:i1585.
6. Gotts JE, Matthay MA. Cell-based therapy in sepsis. a step closer. Am J Respir Crit Care Med. 2018;197:280–1.
7. Bernardo ME, Fibbe WE. Mesenchymal stromal cells: sensors and switchers of inflammation. Cell Stem Cell. 2013;13:392–402.
8. Di Nicola M, Carlo-Stella C, Magni M, Milanesi M, Longoni PD, Matteucci P, et al. Human bone marrow stromal cells suppress T-lymphocyte proliferation induced by cellular or nonspecific mitogenic stimuli. Blood. 2002;99:3838–43.
9. Mezey É. Human mesenchymal stem/stromal cells in immune regulation and therapy. Stem Cells Transl Med. 2022;11:114–34.
10. Burnham AJ, Daley-Bauer LP, Horwitz EM. Mesenchymal stromal cells in hematopoietic cell transplantation. Blood Adv. 2020;4:5877–87.
11. Boregowda SV, Phinney DG. Therapeutic applications of mesenchymal stem cells: current outlook. BioDrugs. 2012;26:201–8.
12. Németh K, Leelahavanichkul A, Yuen PS, Mayer B, Parmelee A, Doi K, et al. Bone marrow stromal cells attenuate sepsis via prostaglandin E(2)-dependent reprogramming of host macrophages to increase their interleukin-10 production. Nat Med. 2009;15:42–49.
13. Liu F, Xie J, Zhang X, Wu Z, Zhang S, Xue M, et al. Overexpressing TGF-β1 in mesenchymal stem cells attenuates organ dysfunction during CLP-induced septic mice by reducing macrophage-driven inflammation. Stem Cell Res Ther. 2020;11:378.
14. Juarez J, Bendall L, Bradstock K. Chemokines and their receptors as therapeutic targets: the role of the SDF-1/CXCR4 axis. Curr Pharm Des. 2004;10:1245–59.
15. Li M, Ransohoff RM. The roles of chemokine CXCL12 in embryonic and brain tumor angiogenesis. Semin Cancer Biol. 2009;19:111–5.
16. Würth R, Bajetto A, Harrison JK, Barbieri F, Florio T. CXCL12 modulation of CXCR4 and CXCR7 activity in human glioblastoma stem-like cells and regulation of the tumor microenvironment. Front Cell Neurosci. 2014;8:144.
17. Chen S, He T, Zhong Y, Chen M, Yao Q, Chen D, et al. Roles of focal adhesion proteins in skeleton and diseases. Acta Pharm Sin B. 2023;13:998–1013.
18. Chen S, Wu X, Lai Y, Chen D, Bai X, Liu S, et al. Kindlin-2 inhibits Nlrp3 inflammasome activation in nucleus pulposus to maintain homeostasis of the intervertebral disc. Bone Res. 2022;10:5.
19. Wu X, Lai Y, Chen S, Zhou C, Tao C, Fu X, et al. Kindlin-2 preserves integrity of the articular cartilage to protect against osteoarthritis. Nat Aging. 2022;2:332–47.
20. Gao H, Zhong Y, Zhou L, Lin S, Hou X, Ding Z, et al. Kindlin-2 inhibits TNF/NF-κB-Caspase 8 pathway in hepatocytes to maintain liver development and function. Elife. 2023;12:e81792.
21. Xu H, Cao H, Xiao G. Signaling via PINCH: functions, binding partners and implications in human diseases. Gene. 2016;594:10–15.
22. Lei Y, Fu X, Li P, Lin S, Yan Q, Lai Y, et al. LIM domain proteins Pinch1/2 regulate chondrogenesis and bone mass in mice. Bone Res. 2020;8:37.
23. Wu X, Chen M, Lin S, Chen S, Gu J, Wu Y, et al. Loss of pinch proteins causes severe degenerative disc disease-like lesions in mice. Aging Dis. 2023;14:1818–33.
24. Gil E, Noursadeghi M, Brown JS. Streptococcus pneumoniae interactions with the complement system. Front Cell Infect Microbiol. 2022;12:929483.
25. Eisen DP, Minchinton RM. Impact of mannose-binding lectin on susceptibility to infectious diseases. Clin Infect Dis. 2003;37:1496–505.
26. Garred P, Pressler T, Lanng S, Madsen HO, Moser C, Laursen I, et al. Mannose-binding lectin (MBL) therapy in an MBL-deficient patient with severe cystic fibrosis lung disease. Pediatr Pulmonol. 2002;33:201–7.
27. Jensenius JC, Jensen PH, McGuire K, Larsen JL, Thiel S. Recombinant mannan-binding lectin (MBL) for therapy. Biochem Soc Trans. 2003;31:763–7.
28. Stanchi F, Bordoy R, Kudlacek O, Braun A, Pfeifer A, Moser M, et al. Consequences of loss of PINCH2 expression in mice. J Cell Sci. 2005;118:5899–910.
29. Ding L, Saunders TL, Enikolopov G, Morrison SJ. Endothelial and perivascular cells maintain haematopoietic stem cells. Nature. 2012;481:457–62.
30. Ding L, Morrison SJ. Haematopoietic stem cells and early lymphoid progenitors occupy distinct bone marrow niches. Nature. 2013;495:231–5.
31. Oertel M, Menthena A, Chen YQ, Shafritz DA. Comparison of hepatic properties and transplantation of Thy-1(+) and Thy-1(-) cells isolated from embryonic day 14 rat fetal liver. Hepatology. 2007;46:1236–45.

32. Zheng D, Oh SH, Jung Y, Petersen BE. Oval cell response in 2-acetylamino-fluorene/partial hepatectomy rat is attenuated by short interfering RNA targeted to stromal cell-derived factor-1. Am J Pathol. 2006;169:2066–74.

33. Ko S, Russell JO, Molina LM, Monga SP. Liver progenitors and adult cell plasticity in hepatic injury and repair: knowns and unknowns. Annu Rev Pathol. 2020;15:23–50.

34. Liu TC, Stappenbeck TS. Genetics and pathogenesis of inflammatory bowel disease. Annu Rev Pathol. 2016;11:127–48.

35. Cao L, Xu H, Wang G, Liu M, Tian D, Yuan Z. Extracellular vesicles derived from bone marrow mesenchymal stem cells attenuate dextran sodium sulfate-induced ulcerative colitis by promoting M2 macrophage polarization. Int Immunopharmacol. 2019;72:264–74.

36. Soontararak S, Chow L, Johnson V, Coy J, Wheat W, Regan D, et al. Mesenchymal stem cells (MSC) derived from induced pluripotent stem cells (iPSC) equivalent to adipose-derived MSC in promoting intestinal healing and microbiome normalization in mouse inflammatory bowel disease model. Stem Cells Transl Med. 2018;7:456–67.

37. Turner MW. Mannose-binding lectin: the pluripotent molecule of the innate immune system. Immunol Today. 1996;17:532–40.

38. Minchinton RM, Dean MM, Clark TR, Heatley S, Mullighan CG. Analysis of the relationship between mannose-binding lectin (MBL) genotype, MBL levels and function in an Australian blood donor population. Scand J Immunol. 2002;56:630–41.

39. Stravalaci M, Pagani I, Paraboschi EM, Pedotti M, Doni A, Scavello F, et al. Recognition and inhibition of SARS-CoV-2 by humoral innate immunity pattern recognition molecules. Nat Immunol. 2022;23:275–86.

40. Tan J, Wu W, Xu X, Liao L, Zheng F, Messinger S, et al. Induction therapy with autologous mesenchymal stem cells in living-related kidney transplants: a randomized controlled trial. JAMA. 2012;307:1169–77.

41. Panés J, García-Olmo D, Van Assche G, Colombel JF, Reinisch W, Baumgart DC, et al. Expanded allogeneic adipose-derived mesenchymal stem cells (Cx601) for complex perianal fistulas in Crohn's disease: a phase 3 randomised, double-blind controlled trial. Lancet. 2016;388:1281–90.

42. Leng Z, Zhu R, Hou W, Feng Y, Yang Y, Han Q, et al. Transplantation of ACE2(-) mesenchymal stem cells improves the outcome of patients with COVID-19 pneumonia. Aging Dis. 2020;11:216–28.

43. Li P, Ou Q, Shi S, Shao C. Immunomodulatory properties of mesenchymal stem cells/dental stem cells and their therapeutic applications. Cell Mol Immunol. 2023;20:1–12.

44. Giri J, Das R, Nylen E, Chinnadurai R, Galipeau J. CCL2 and CXCL12 derived from mesenchymal stromal cells cooperatively polarize IL-10+ tissue macrophages to mitigate gut injury. Cell Rep. 2020;30:1923–.e1924.

45. Gonzalez-Rey E, Anderson P, González MA, Rico L, Büscher D, Delgado M. Human adult stem cells derived from adipose tissue protect against experimental colitis and sepsis. Gut. 2009;58:929–39.

46. Logan M, Martin JF, Nagy A, Lobe C, Olson EN, Tabin CJ. Expression of Cre Recombinase in the developing mouse limb bud driven by a Prxl enhancer. Genesis. 2002;33:77–80.

47. Liu H, Li P, Zhang S, Xiang J, Yang R, Liu J, et al. Prrx1 marks stem cells for bone, white adipose tissue and dermis in adult mice. Nat Genet. 2022;54:1946–58.

48. Seita J, Weissman IL. Hematopoietic stem cell: self-renewal versus differentiation. Wiley Interdiscip Rev Syst Biol Med. 2010;2:640–53.

49. Boulais PE, Frenette PS. Making sense of hematopoietic stem cell niches. Blood. 2015;125:2621–9.

50. Xiao G, Cheng H, Cao H, Chen K, Tu Y, Yu S, et al. Critical role of filamin-binding LIM protein 1 (FBLP-1)/migfilin in regulation of bone remodeling. J Biol Chem. 2012;287:21450–60.

51. Budgude P, Kale V, Vaidya A. Cryopreservation of mesenchymal stromal cell-derived extracellular vesicles using trehalose maintains their ability to expand hematopoietic stem cells in vitro. Cryobiology. 2021;98:152–63.

52. Imai Y, Nakagawa S, Ito Y, Kawano T, Slutsky AS, Miyasaka K. Comparison of lung protection strategies using conventional and high-frequency oscillatory ventilation. J Appl Physiol. 2001;91:1836–44.

53. Dieleman LA, Palmen MJ, Akol H, Bloemena E, Peña AS, Meuwissen SG, et al. Chronic experimental colitis induced by dextran sulphate sodium (DSS) is characterized by Th1 and Th2 cytokines. Clin Exp Immunol. 1998;114:385–91.

54. He T, Shang J, Gao C, Guan X, Chen Y, Zhu L, et al. A novel SIRT6 activator ameliorates neuroinflammation and ischemic brain injury via EZH2/FOXC1 axis. Acta Pharm Sin B. 2021;11:708–26.

55. Kim JJ, Shajib MS, Manocha MM, Khan WI. Investigating intestinal inflammation in DSS-induced model of IBD. J Vis Exp. 2012;1:3678.

ACKNOWLEDGEMENTS

AUTHOR CONTRIBUTIONS

Study design: GX, TH, BZ, GS, XB and HC. Study conduct and data collection: TH, ZB, GS, YL, QY, SL, GM, WJ, XW, YZ, DG, QY, TC and GX. Data analysis: TH, BZ, HC and GX. Data interpretation: GX, CL, TH, SH, TC, XB and DC. Drafting the manuscript: GX and TH. TH, HC and GX take the responsibility for the integrity of the data analysis.

COMPETING INTERESTS

The authors declare no competing interests.

ETHICS

The animal experiments conformed to the guidelines and regulatory standards of the Institutional Animal Care and Use Committee (IACUC) at the Southern University of Science and Technology, No. SUSTC-JY2019153.

ADDITIONAL INFORMATION

Supplementary information The online version contains supplementary material available at https://doi.org/10.1038/s41418-023-01243-9.

Correspondence and requests for materials should be addressed to Xiaochun Bai, Tao Cheng, Huiling Cao or Guozhi Xiao.

Reprints and permission information is available at http://www.nature.com/reprints

Publisher's note Springer Nature remains neutral with regard to jurisdictional claims in published maps and institutional affiliations.